CHALMERS

UNIVERSITY OF TECHNOLOGY

Influence of support properties on the hydrodeoxygenation of a lignin model compound over NiMo catalysts

Master's thesis within the Innovative and Sustainable Chemical Engineering programme

SIMON PEKKARI

Department of Chemistry and Chemical Engineering
CHALMERS UNIVERSITY OF TECHNOLOGY
Gothenburg, Sweden 2019

Influence of support properties on the hydrodeoxygenation of a lignin model compound over NiMo catalysts

SIMON PEKKARI

Influence of support properties on the hydrodeoxygenation of a lignin model compound over NiMo catalysts
SIMON PEKKARI

Supervisors:
Derek Creaser, Department of Chemistry and Chemical Engineering
Muhammad Abdus Salam, Department of Chemistry and Chemical Engineering
Jung Won Woo, Department of Chemistry and Chemical Engineering

Examiner:
Louise Olsson, Department of Chemistry and Chemical engineering

Influence of support properties on the hydrodeoxygenation of a lignin model compound over NiMo catalysts

SIMON PEKKARI
Department of Chemistry and Chemical Engineering
Chalmers University of Technology

Abstract

Environmental challenges such as increasing greenhouse gas emissions have intensified the need for sustainable chemicals and fuels. Hydrodeoxygenation (HDO) is a technique for upgrading bio-based feedstocks to renewable chemicals and fuels. To meet the increased need for these sustainable products, new raw materials are needed. Lignin, which is one of the major constituents of woody plants, has shown to be a promising raw material for renewable chemicals and fuels. In this thesis, bifunctional catalysts consisting of nickel and molybdenum (NiMo) supported on Y zeolites with different properties is used for HDO of a model compound that represents a structural unit of lignin.

The main objective of the thesis was to investigate how support properties influence the activity, selectivity and rate of deactivation of the catalysts. Bifunctional catalysts were synthesized by impregnating NiMo on Y zeolites with different Si/Al ratios. One zeolite was further exposed to a surfactant-assisted post-treatment to introduce secondary mesoporosity. The catalysts were characterized by nitrogen physisorption, X-Ray Diffraction (XRD) and ammonia temperature programmed desorption (TPD). Reaction experiments were conducted in a batch reactor at 320 and 345 °C with 50 bar hydrogen pressure. Product samples were collected during the experiments and analyzed by gas chromatography mass spectrometry (GC-MS) to evaluate the activity and selectivity. The spent catalysts were analyzed by elemental microanalysis to determine the coke deposition.

The results indicate that bifunctional catalysts of NiMo and Y zeolite can effectively cleave ether and relatively strong C-C linkages. The support properties such as pore structure and acidity seem to have a great impact on selectivity and activity of the catalysts. The acidity seems to have the greatest impact on HDO performance. Moreover, the results indicate that the presence of secondary mesoporosity increases the selectivity towards dimer formation. It seems that the catalyst supported on Y zeolite with a Si/Al of 15 shows the best HDO performance. Lastly, the results also indicate that support properties affect the rate of coke formation, it seems both acidity and pore structure has an impact on the coking mechanism.

Acknowledgements

Contents

List of Abbreviations

BET   Brunauer-Emmett-Teller

BJH   Barrett-Joyner-Halenda

CTAB   Cetyl trimethylammonium bromide

DA   Deoxygenated aromatics

DDO   Direct deoxygenation

DMDS   Dimethyl disulfide

DME   Demethylation

DMO   Demethoxylation

DSC   Differential scanning calorimeter

FID   Flame ionization detector

GC   Gas chromatography

HDM   Hydrodemetallization

HDN   Hydrodenitrogenation

HDO   Hydrodeoxygenation

HDS   Hydrodesulfurization

HYD   Hydrogenation

M-Y15   Modified Zeolyst CBV720

MFC   Mass flow controller

MS   Mass spectrometry

PEP   Phenethylphenol

PPE   2-Phenethyl phenyl ether

TCD   Thermal conductivity detector

TPD   Temperature programmed desorption

Y15   Zeolyst CBV720

Y2.6   Zeolyst CBV300

Y40   Zeolyst CBV780

List of Figures

List of Tables

1

Introduction

1.1 Background

Today the world is facing a severe challenge with the increasing amount of greenhouse gas emissions and fossil fuel depletion due to increasing demands worldwide [1]. The transport sector is responsible for a large amount of the CO_2 emissions and with a growing population the need for fuels will most likely increase in the future [1, 2]. Biofuels are expected to play a crucial role as substitutes for fuels produced from crude oil to significantly reduce CO_2 emissions [2]. Biofuels produced from biomass are believed to be CO_2 neutral since the biomass absorbs the same amount of CO_2 when it grows as when the biofuel is consumed [3].

Biofuels can be produced from several different feedstocks and are divided into three different generations. Two main first-generation biofuels are bioethanol and biodiesel. These fuels have a major drawback, they are produced from food crops and thus, they compete with food production. Second-generation biofuels are produced from feedstocks that are non-edible and therefore do not compete with food production. Some examples of second generation feedstocks are waste oils, forest residue and lignocellulosic feedstocks. In recent years a third generation has also emerged that focuses on the production of biofuels from microscopic organisms such as algae [3].

Bio-based feedstocks contain large amounts of oxygen and therefore have a low heating value [1]. Hydrodeoxygenation (HDO) is a process where these feedstocks are treated with hydrogen over a catalyst under high temperature and pressure to remove oxygen. HDO of triglyceride-based feeds such as vegetable oil, tall oil and other waste oils into advanced diesel fuels have been extensively studied. It can be performed in co-processing units where the renewable feed is mixed with petroleum-based feeds and in stand-alone units with 100% renewable feeds [4]. Commercial processes performing HDO of such feeds are e.g Haldor Topsøe's HydroFlex™and Neste's NExBTL [5, 6].

The increasing interest and demand for biofuels have led to an extensive search for new raw materials for biofuel production. Lignocellulosic biomass consists of mainly cellulose, hemicelluloses and lignin. Lignin is today underutilized and has proven

to be an interesting potential source of biofuels and chemicals. The pulp and paper industry generates large amounts of lignin which is mostly burned in industrial boilers to produce energy. Due to increased energy efficient plant design, modern pulp and paper mills have a surplus of energy, which makes it possible to extract lignin without affecting the process. In recent years the valorization of lignin has been extensively studied and HDO of lignin or lignin-derived bio-oil has shown great potential for the production of renewable chemicals and fuels. The lignin structure is, however, very complex and heterogeneous which complicates the development of a suitable catalyst [7, 8].

Traditional petrochemical hydrotreating catalysts, such as metal sulfides supported on gamma alumina (γ-Al_2O_3) have been successfully used for HDO of several different biomass feedstocks [1]. When treating lignin however, several challenges arise due to its complexity and high content of strong carbon-carbon linkages [9]. To improve the performance of these catalysts, different support materials have been investigated to replace γ-Al_2O_3. Y zeolite is a faujasite with great cracking capability due to its high Brønsted acidity, it shows great potential as a catalyst support due to its high surface area allowing it to produce a high dispersion of the active phase [10].

1.2 Aim

This thesis aims to investigate how different catalyst support properties influence the HDO performance of a sulfided NiMo catalyst when treating a lignin model compound, 2-Phenethyl phenyl ether (PPE). In this study bifunctional catalysts consisting of NiMoS, a catalyst known to be active for deoxygenation reactions is to be combined with Y zeolite, a typical hydrocracking catalyst.

Three commercial Y zeolites produced by Zeolyst International with varying Si/Al ratio is to be used, CBV300 (Si/Al of 2.55), CBV720 (Si/Al of 15) and CBV780 (Si/Al of 40). These zeolites have varying properties such as pore structure and acidity. CBV720 will be modified by a post-treatment to introduce secondary mesoporosity to further investigate how the support pore structure influences the HDO performance.

Important questions to be answered by the results of this thesis are:

- How is the activity and product selectivity of the catalyst influenced by support properties?

- How is the rate of coking influenced by support properties?

- Is there an optimal Si/Al ratio with a good balance of activity, selectivity and coke formation?

2

Theoretical background

In this chapter relevant theory for the thesis is presented. The chapter aims to give an understanding of the complexity of the raw material and theoretical insight into the process of catalytic HDO. The chapter also aims to introduce the reader to different catalysts used for HDO in previous research.

2.1 Lignin

Lignin is the second most abundant biopolymer found in nature behind cellulose. It is found in plant cell walls where it fills the voids between cellulose and hemicelluloses and acts as a glue to hold the lignocellulosic material together. Lignin is a complex three-dimensional macromolecule consisting of phenylpropane units and is considered to be the only abundant source of aromatics found in nature [7]. The lignin polymer mainly consists of three types of monomers called monolignols, which include: coniferyl alcohol, p-coumaryl alcohol and sinapyl alcohol (see Figure 2.1) that are linked together by C-O-C (ether) and C-C (carbon-carbon) bonds [7, 11]. All of these monomers contain a phenyl group and a propyl side chain and thus are called phenylpropane units [7].

Sinapyl alcohol   **Coniferyl alcohol**   **p-Coumaryl alcohol**
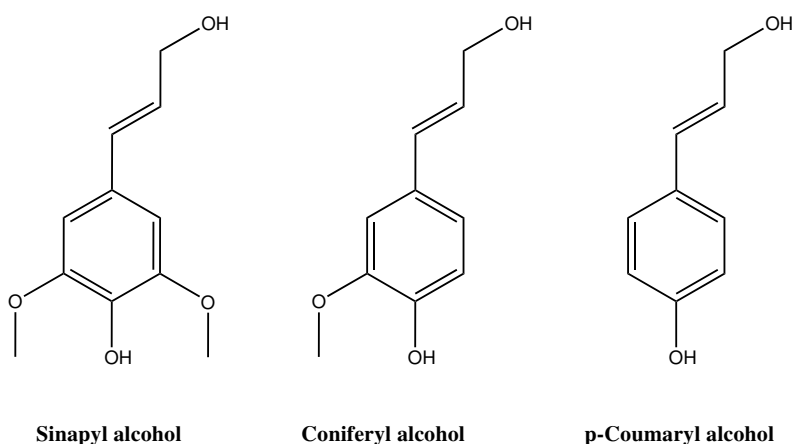
Figure 2.1: Monolignols, the primary building blocks of lignin.

The linkages between the phenylpropane units in lignin consists mainly of β-O-4 (β-aryl-ether), β-β (resinol) and β-5 (phenylcoumaran) and a smaller amount of α-O-4

(α-aryl-ether), 4-O-5 (diaryl ether) and 5-5' bonds [7]. The β-O-4 bond, however, is by far the most common linkage and represent about 50 % of the total linkages in native lignin [11].

2.1.1 Technical lignins

So called technical lignins are produced as by-products in large quantities in lignocellulosic refineries such as kraft, soda and sulfite pulp mills. Today, the kraft process is the most common chemical pulping process, it constitutes roughly 85 % of the total lignin production in the world. During kraft pulping, lignin is removed from the wood through treatment with a liquor containing sodium hydroxide and sodium sulfide. The lignin polymer is degraded into smaller fragments that are soluble in the alkali solution [7]. Most of the lignin is today incinerated in boilers to produce steam and energy for the pulp mills. However, in modern mills, the energy produced through incineration is in surplus, which makes it possible to extract a large portion of the kraft lignin for conversion into higher value products without interfering with the process [7, 12].

The chemical structure of kraft lignin differs from that of native lignin, it contains a larger amount of phenolic hydroxyl groups and condensed structures such as biphenyl. The kraft lignin also contains an increased amount of carboxyl groups and the oxidative conditions in the process can lead to the formation of catechol and quinine structures [7, 12, 13]. The sulfides employed during the process also leads to small amounts of sulfur ending up in the kraft lignin [12].

2.1.2 Lignin model compounds

Due to the complex structure of the lignin polymer and its derivatives the use of lignin model compounds with lower molecular mass have been extensively used in research. The model compounds contain building blocks and linkages found in the lignin polymer but, circumvent the variability and its insolubility in most organic solvents. These compounds are therefore useful for more controlled research studies to gain mechanistic insights into lignin valorization. Several different lignin model compounds have been used in earlier research including monomeric phenolics such as phenol, cresol, anisole and guaiacol since they are found in lignin derived bio-oil. Dimers containing two aromatic units linked together by C-O or C-C bonds such as β-O-4, α-O-4, 4-O-5 or 5-5' have also been used since they mimic the bonds found in the lignin polymer [7, 14]. Figure 2.2 shows some commonly used lignin model compounds.
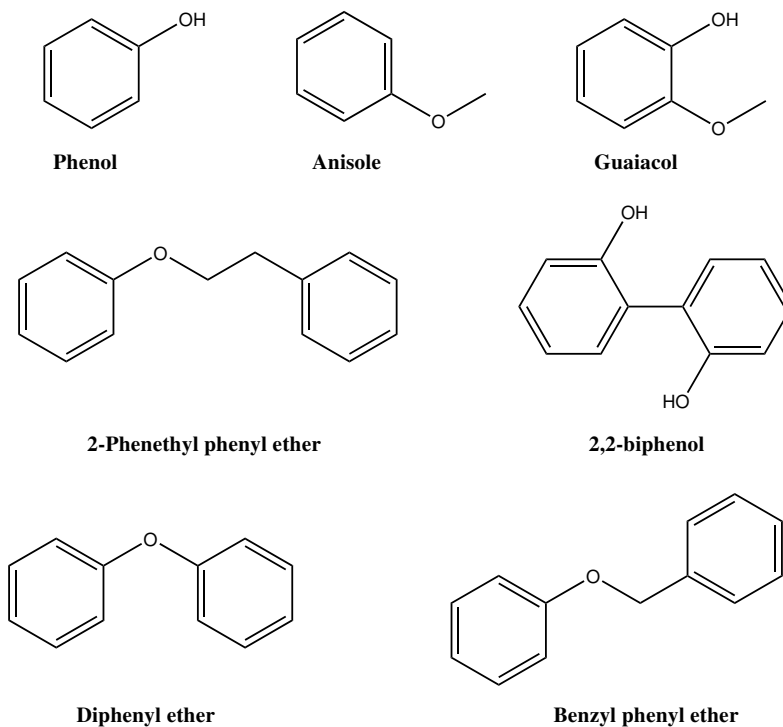
Figure 2.2: Examples of lignin model compounds that mimic fragments and linkages found in lignin [15–17].

2-Phenethyl phenyl ether (PPE) is a dimeric lignin model compound containing one of the most common ether linkages within lignin, the β-O-4 bond [18]. PPE will be used as the model compound for this thesis.

2.2 Hydrodeoxygenation process

Hydrotreating processes are performed in refineries all over the world to upgrade fossil petroleum fractions into high quality fuels. These hydrotreating processes involve reactions such as hydrodesulfurization (HDS), hydrodenitrogenation (HDN), hydrodemetallization (HDM) and hydrodeoxygenation (HDO). These reactions use high pressure hydrogen over a heterogeneous catalyst to remove sulfur, oxygen, metal and nitrogen heteroatoms from the petroleum feedstocks by hydrogenolysis [19].

Since fossil feedstocks contain only small amounts of oxygen it has been paid less attention to HDO compared to HDS and HDN in the earlier petroleum upgrading research [4]. The purpose of HDO is to upgrade renewable feedstocks by reducing the oxygen content. Biomass and bio-oils contain high amounts of various oxygenated functional groups and therefore, have a low heating value and low chemical stability compared to fossil oils [1]. The HDO route of biomass is considered to involve a complex reaction network and the reactions depend on the type of biomass feedstock. The main reaction is hydrodeoxygenation where oxygen is removed in the form of water by C-O bond cleavage. The reaction can be generally expressed as shown in

Equation 2.1 [1, 20].

Hydrodeoxygenation:

$$R-OH + H_2 \longrightarrow R-H + H_2O \tag{2.1}$$
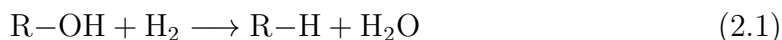
Several other reactions are involved during HDO such as hydrocracking, hydrogenation, decarboxylation and decarbonylation. The reactions are adopted from Mortensen et al. and are summarized in Equations 2.2-2.5 [1].

Hydrogenation:

$$R_1-HC=CH-R_2 + H_2 \longrightarrow R_1-CH_2-CH_2-R_2 \tag{2.2}$$

Hydrocracking:

$$R_1-CH_2-CH_2-R_2 + H_2 \longrightarrow R_1-CH_3 + H_3C-R_2 \tag{2.3}$$

Decarboxylation:

$$R-COOH \longrightarrow R-H + CO_2 \tag{2.4}$$

Decarbonylation:

$$R-COOH + H_2 \longrightarrow R-H + CO + H_2O \tag{2.5}$$
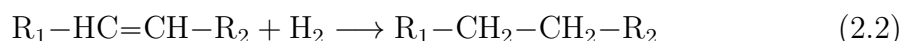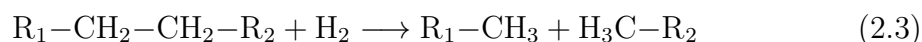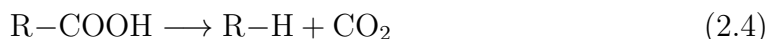
2.2.1 HDO of Lignin model compounds

HDO of lignin is considered very complex and several pathways have been suggested. The reaction pathway depends on the model compound and the catalyst employed. Reports from literature suggests that two major routes occur in parallel during HDO of monomeric model compounds such as phenol, anisole and guaiacol. The first route is direct deoxygenation (DDO) to form aromatic compounds and the second route is hydrogenation of the aromatic ring (HYD), followed by removal of oxygen through hydrodeoxygenation [8, 14]. Removal of methoxy groups from the phenolic compounds can also occur by C-O bond cleavage through demethylation (DME) and demethoxylation (DMO) [8]. Phenol is the simplest monomeric lignin model compound, two suggested reaction pathways for HDO of phenol over a metal sulfide or noble metal catalyst is shown in Figure 2.3.
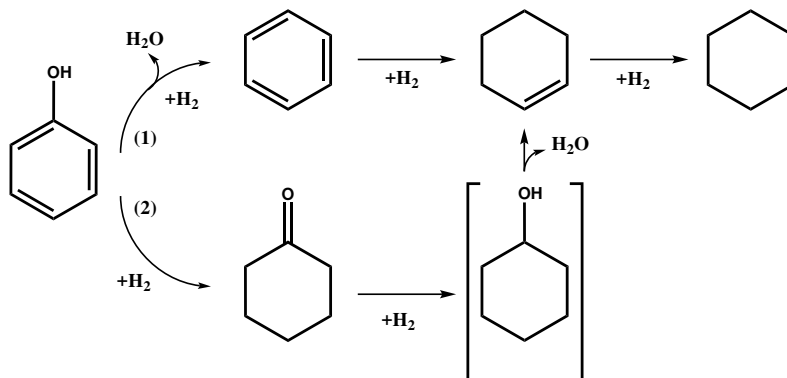
Figure 2.3: Proposed pathways for HDO of phenol over a metal sulfide or noble metal catalyst. The figure is drawn on the basis of information from Saidi et al. [8].

The first pathway involves direct deoxygenation to produce benzene and further hydrogenation to give cyclohexane. In the second pathway phenol is converted into cyclohexanone, which is further hydrogenated into cyclohexanol. The cyclohexanol is then deoxygenated to give cyclohexane. What reaction pathway is favored depends on the catalyst. Güvenatam et al. studied HDO of phenol in aqueous phase over noble metal catalysts supported on carbon and γ-Al$_2$O$_3$. The reactions proceeded predominantly through the second pathway resulting in mainly cyclohexanone and cyclohexane as products [15]. However, Senol et al. have reported that when using metal sulfide catalysts supported on γ-Al$_2$O$_3$ when treating phenol in m-xylene the products consist of both benzene, cyclohexanone and cyclohexanol, which suggests that the catalyst is active for both pathways [21].

Dimeric lignin model compounds have been used to investigate the cleavage of lignin linkages under HDO conditions. Several studies show that the β-O-4, α-O-4 and 4-O-5 bonds can be cleaved under HDO conditions using different catalysts [9, 15, 22]. Carbon-carbon linkages are however, harder to break under these conditions. Jongerius et al. treated 2,2-biphenol, a dimer containing the 5-5' linkage at 300 °C with 50 bar of hydrogen over a sulfided CoMo/Al$_2$O$_3$ catalyst for 4 h and all products still contained the 5-5' linkage [9]. Güvenatam et al. have also reported that when treating diphenyl methane, a dimer containing the β-1 linkage and biphenyl containing the 5-5' linkage over a Pt/C catalyst the C-C bonds are not cleaved [15]. This suggests that to effectively depolymerize and deoxygenate lignins with a high content of C-C linkages such as technical lignins a catalyst with both good cracking and HDO capability must be developed.

2.3 Catalysts

The development of efficient catalysts for lignin HDO is today an active area of research. The goal of this research is to gain deeper mechanistic insights in how various catalyst functions affect the activity, selectivity and rate of deactivation [8]. The use of several different catalysts have been reported in the literature, these catalysts consist of supported transition and noble metals such as palladium (Pd), platinum (Pt), ruthenium (Ru), copper (Cu), molybdenum (Mo), cobalt (Co) and nickel (Ni) [15, 16, 23]. The noble metal catalysts have shown great activity for HDO of lignin model compounds in previous studies [15]. However, the high cost of these noble metals hinders their use in large scale industrial processes. Noble metal catalysts are also very sensitive to sulfur poisoning, which can hinder their use for processing sulfur containing lignins such as kraft lignin and lignosulphonates. [16, 23, 24].

The higher availability and lower cost of transition metals have shifted large focus towards using supported mono- or bimetallic catalysts. Sulfided bimetallic catalysts such as NiMoS$_2$ and CoMoS$_2$ are the most frequently studied catalysts for HDO since these catalysts have been extensively used in the traditional hydrotreating processes [1, 15, 25]. In these sulfided catalysts active sites are generated through interactions

between the two metals. Nickel and cobalt are promoters that donate electrons to the molybdenum atoms, which weakens the bond between molybdenum and sulfur, which further generates a vacancy site that is active for HDO. Mortensen et al. have proposed a mechanism for HDO of 2-ethylphenol over a sulfided CoMo catalyst, which is illustrated in Figure 2.4. The oxygen in 2-ethylphenol is believed to adsorb on the active site and by proton donation from the sulfur a carbocation is formed. This carbocation can then undergo direct deoxygenation to form ethylbenzene and the bound oxygen is then removed in the form of water [1].
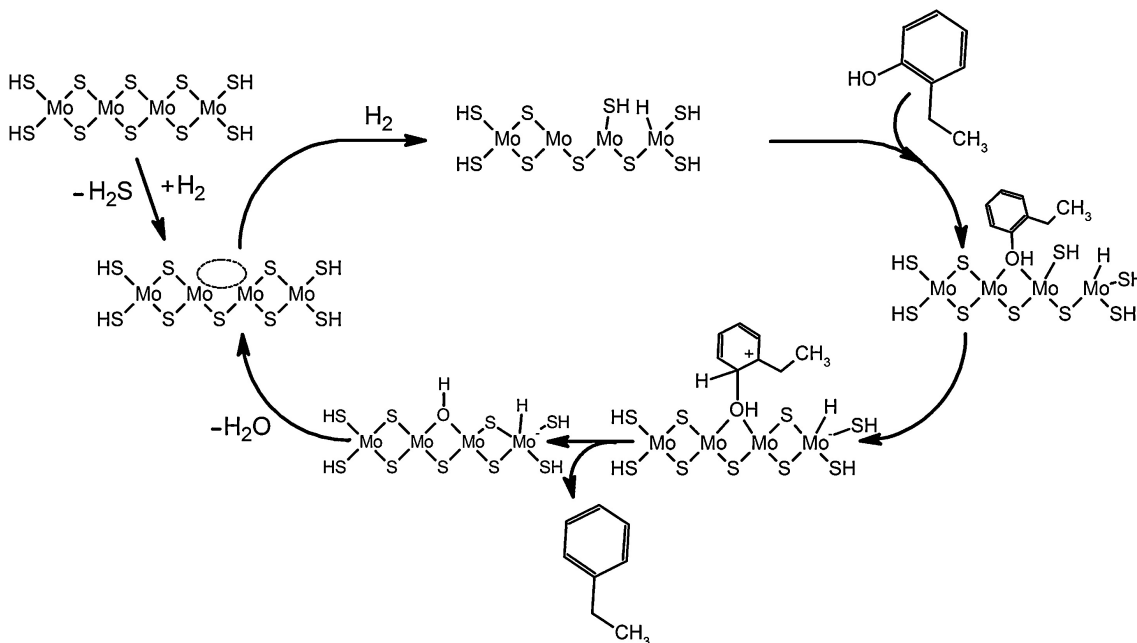
Figure 2.4: A suggested reaction mechanism of the DDO pathway of 2-ethylphenol over a sulfided $CoMoS_2$ catalyst [1].

As mentioned, studies on HDO of monomeric lignin model compounds catalyzed by metal sulfides have shown great potential for oxygen removal. The use of metal sulfide catalysts for HDO of lignin has, however, also raised some concerns due to the potential sulfur contamination of products and loss of activity [8, 9]. Senol et al. reported that when performing HDO of phenol using metal sulfides, trace amounts of cyclohexanethiol was detected as a product [21]. When the sulfided catalysts are used for HDS they are kept in the sulfide form by the high concentration of H_2S in the surrounding environment. This suggests that if the biomass feedstock does not contain enough sulfur, an extra sulfur source could be needed to prevent deactivation [8].

2.3.1 Supports

The purpose of a catalyst support is to stabilize the active catalytic material in a highly dispersed form [8]. The support material plays an important role and can alter the activity and selectivity of the catalyst. Properties of the support such as pore structure, surface area and acidity greatly affect the performance of the catalyst [26]. The support material can contain solid acids in the form of Brønsted and Lewis acid sites, the acid properties of the support can affect the product distribution in HDO of bio-oil. Active acid sites in the support material can catalyze certain reactions and thus, make the catalyst bifunctional [16].

Acid sites can catalyze transalkylation reactions, where alkyl groups in compounds such as anisole are transferred from the alkoxy group to the phenolic ring. [27]. Wang et al. have proposed a reaction pathway for the transalkylation of anisole over a bifunctional NiMo catalyst with an acidic function. As explained in Figure 2.5, the C-O bond in ansiole is first cleaved through demethylation to form a carbenium ion. The reaction then proceeds by acid catalyzed alkylation of the carbenium ion onto the aromatic ring to produce cresol [28].
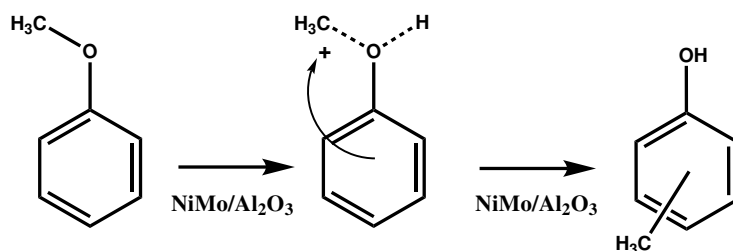
Figure 2.5: A suggested reaction pathway for the transalkylation of anisole over a bifunctional NiMo catalyst. The figure is drawn on the basis of information from Wang et al. [28].

Cracking reactions where C-C linkages are cleaved can also be catalyzed by acid sites. The catalytic cracking mechanism of an alkane is described in Figure 2.6. Catalytic cracking over Brønsted acid sites is initiated by the formation of a carbocation, which is formed through proton donation by the Brønsted acid site to the alkane. The reaction proceeds by C-C bond cleavage through either β-scission or α-scission where the former is the most thermodynamically favoured and therefore accounts for the majority of the cracking. The β-scission produces an alkene and another carbocation, which continues the cracking reactions until the carbocation is desorbed from the active acid site, and hydrogen transfer from the carbocation to the Brønsted acid site restore it to its original state [29].
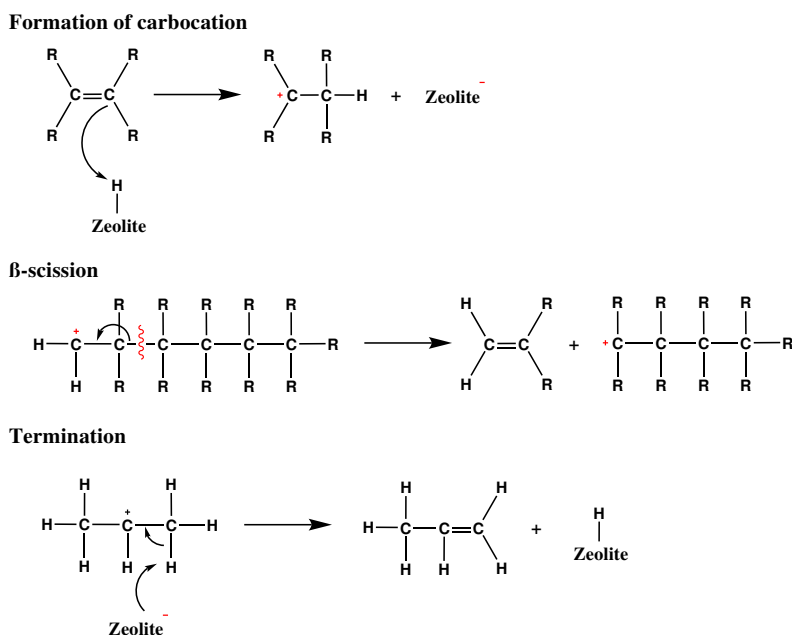
Figure 2.6: Suggested reactions responsible for cracking an alkane over a Brønsted acid site in zeolite. The figure is drawn on the basis of information from Komvokis et al. [29].

The most commonly used catalyst support for hydrotreating catalysts is gamma alumina (γ-Al_2O_3) due to its good textural and mechanical properties as well as low cost [30]. However, γ-Al_2O_3 suffers from some drawbacks, large amounts of water which can be present during HDO might convert it into boehmite (AlO(OH)), which can further deactivate the catalyst. The relatively high acidity of γ-Al_2O_3 also makes it more prone to deactivate by coking. Silica (SiO_2) has been suggested as an alternative support for HDO. Silica is relatively inert and has a low acidity and therefore, shows low affinity for carbon formation [1]. Another promising support is activated carbon, the carbon support is more stable when exposed to water and shows negligible coke formation during HDO of bio-oil [31]. However, the carbon support has extensive microporosity, which makes it unsuitable for treating larger molecules [30]. Titania (TiO_2) and zirconia (ZrO_2) have also successfully been used as supports for HDO of bio-oil, the materials are less acidic and more tolerable to water compared to γ-Al_2O_3 making them less prone to deactivation. These materials have, however, much lower surface area [32, 33].

2.3.1.1 Y Zeolite

Faujasite zeolites are also mentioned as potential supports for HDO catalysts in the literature. These zeolites are aluminosilicates with high surface area, shape selectivity and the ability to produce high dispersion of the active metals [10, 30]. Y zeolite is a faujasite that is commonly used in the petrochemical industry both as an active catalyst and catalyst support. The good hydrothermal stability and Brønsted acidity of the support makes it highly suitable for catalytic cracking applications [10].

Y zeolite has a Si/Al molar ratio of 2.5 and contains a three-dimensional network of micropores (<1 nm in diameter) [34].

The presence of micropores in Y zeolite may result in a reduced transport rate of bulky substrates and therefore, reduce the effectiveness factor of the catalyst [10]. In order to reduce the diffusion limitations and improve the performance, several approaches of introducing mesopores (2-50 nm in diameter) into the material have been studied. The different approaches can be categorized into two different categories, top-down and bottom-up approaches. The bottom-up approaches are primarily syntheses where mesopores are formed by templates when the zeolite material is produced. Surfactants, polymers and starch are examples of templates that have been used [35]. The top-down approaches are typically post-treatments where one of the main components are partly removed, either silicon is removed by desilication or aluminum by dealumination [36].

Stabilization of pristine Y zeolite by dealumination is performed in industry through steam treatment and subsequent acid leaching resulting in a so called ultra-stable zeolite (USY zeolite). The treatment results in a zeolite with less Al (higher Si/Al ratio), higher hydrothermal stability and larger cavities in the form of mesopores. The dealumination can be performed to a varying extent making it possible to tune the acidity and mesoporosity of the zeolite [35, 37]. In zeolites, Brønsted acid sites are generated by weakly bound protons in hydroxyl groups bridging framework silicon and aluminum atoms. By varying the Si/Al ratio of the zeolite both the amount as well as strength of the Brønsted acid sites are altered. Zeolites with low Si/Al ratio are believed to have many but weak acid sites whilst zeolites with high Si/Al ratio have relatively few acid sites but with a higher acid strength [38, 39]. Some research is however, suggesting that some of the mesopores in USY zeolite are present as cavities connected through micropores and thus not improving the diffusion of large molecules to a very large extent [35].

A new and promising top-down approach is the surfactant-templated post-synthetic modification. This approach is a single-step treatment where USY zeolite is treated with a surfactant in a mildly basic solution to introduce secondary mesoporosity. Mostly Cetyl trimethylammonium bromide (CTAB) has been used as the templating surfactant [35]. García-Martínez et al. first described this technique and they successfully introduced secondary mesoporosity into a commercial USY zeolite (Zeolyst CBV720) [36]. The mesoporosity is suggested to be introduced through crystal-rearrangement. The basic solution opens $Si-O-Si$ bonds in the zeolite to form charged $Si-O^-$ species. The cationic surfactant then interacts with these species and forms micelles, then crystal rearrangement occurs to accommodate the surfactant micelles. By further treatment the surfactant template is removed and the formed mesopores are exposed [35, 36].

2.3.2 Catalyst deactivation

Catalyst deactivation is a major economical concern in large scale hydrotreating processes. Stopping the production to replace the catalyst is a very costly operation both due to the cost of the catalytic material but also due to the loss of revenue during the shutdown. In the HDO process catalyst deactivation occurs in several ways, including deposition of carbonaceous species (coking), poisoning of active sites by different compounds and sintering. The main cause of deactivation in HDO catalysts is coking. Coke depositions may both cover active sites and block whole pores, greatly reducing the active surface of the catalyst [8].

Coke is formed through two main reactions, polymerization and polycondensation. The rate of these reactions depends on the nature of the feed, the catalyst properties and the operating conditions. Aromatics, alkenes and heterocyclics are more prone to coke formation then other saturated hydrocarbons due to their stronger interaction with the catalyst surface. The Lewis and Brønsted acidity of the catalyst also affects coke formation. Coking increases with increased acidity and since the acidity also helps catalyze HDO and hydrocracking a tradeoff between a high rate of coking and good deoxygenation and depolymerization arises. Process conditions such as hydrogen partial pressure and temperature also influence the coke formation, if the partial pressure is high enough hydrogen can turn coke precursors into more stable products before they are converted into coke [8, 40].

Catalyst poisons can adsorb on the active catalytic sites and reduce the activity by either competing for active sites with the reactants or by completely occupying the active sites. Poisons can either be adsorbed reversibly or irreversibly. A reversible poison is only temporarily adsorbed on the active site and will desorb when the poison is removed from the feed. An irreversible poison, however, is bound so strongly that it will not desorb once adsorbed on the surface and the catalyst activity will remain reduced [40].

3

Experimental methods

This chapter describes the experimental methods employed during the thesis. The first part explains how the catalysts were prepared and characterized and the second part gives an in depth description of the HDO experiments.

3.1 Catalyst preparation

Bifunctional NiMo catalysts were prepared using four different Y zeolite supports from Zeolyst International with different Si/Al molar ratios: CBV300 (Si/Al of 2.55), CBV720 (Si/Al of 15), CBV780 (Si/Al of 40) and a modified CBV720. The CBV720 support was modified using the method described in Section 3.1.1. The Y zeolites will hereafter be referred to as described in Table 3.1.

Table 3.1: Abbreviations of the Y zeolites used in the study.

Material	Si/Al	Abbreviation
CBV300	2.55	Y2.6
CBV720	15	Y15
Modified CBV720	15	M-Y15
CBV780	40	Y40

3.1.1 Surfactant-assisted modification of USY zeolite

Commercial USY zeolite, Y15 was modified using a surfactant template approach [36]. 1.4 g of CTAB was dissolved in 128 mL of 0.37 M NH_4OH solution and stirred for 1 h. 2 g of USY zeolite was then added to the mixture and stirred for 20 min. The mixture was then transferred into a 300 mL Parr instruments autoclave and heated to 150 °C in air under autogenous pressure for 10 h. The mixture was then transferred into plastic tubes and centrifuged. The solid was then washed with deionized water and then centrifuged again, this was repeated 5 times. The resulting solid was then dried at 90 °C for 20 h. Further, the dried solid was grounded and calcined at 550 °C (with a temperature ramp of 5 °C/min) for 8 h.

3.1.2   Wet impregnation

The catalysts were loaded with nickel and molybdenum using a sequential impregnation method. The target metal loading of the catalysts were 15 wt% molybdenum and 5 wt% nickel. Prior to impregnation the support material was calcined at 550 °C for 6 h (with a temperature ramp of 5 °C/min). In a typical impregnation procedure, approximately 3 g of support material was mixed with 50 mL deionized water and stirred. The pH of the mixture was adjusted to 4 by adding nitric acid drop-wise. Molybdenum oxide precursor ($(NH_4)_6Mo_7O_{24} \cdot 4H_2O$) was then mixed with 20 mL deionized water and added drop-wise to the support-mixture and then left under stirring for 30 min. The pH was maintained at 4 by adding nitric acid drop-wise during this period. The molybdenum mixture was then transferred to a round bottom flask and freeze-dried overnight to remove moisture and then calcined at 450 °C for 2 h (with a temperature ramp of 5 °C/min).

The prepared sample was then further mixed with 50 mL deionized water and stabilized at pH 9 by adding a solution of ammonium hydroxide drop-wise. Nickel nitrate precursor ($(Ni(NO_3)_2 \cdot 6H_2O$) was then mixed with 20 mL deionized water and added drop-wise to the molybdenum mixture while maintaining the pH at 9. Further, the resulting mixture was freeze-dried overnight and calcined at 450 °C for 2 h (with a temperature ramp of 5 °C/min).

3.2   Catalyst characterization

3.2.1   Nitrogen physisorption

The specific surface area, pore volume and pore size distribution of the catalysts and catalyst support materials were evaluated by nitrogen physisorption. The analysis was performed at 78K in a Micromeritics TriStar 3000 instrument. Prior to analysis the samples were degassed at 250 °C in a nitrogen atmosphere for 6 h in order to remove any impurities adsorbed on the surface.

The specific surface area was calculated by the Brunauer-Emmett-Teller equation (BET), Equation 3.1 [41]. The microporous volume was calculated using the t-plot method and the total pore volume was calculated from the amount of nitrogen adsorbed at a relative pressure of $P/P_0 = 0.99$. The mesoporous volume was then calculated by subtracting the microporous volume from the total pore volume. The pore size distribution was determined according to the Barrett-Joyner-Halenda method (BJH) based on the adsorption branch of each isotherm.

$$\frac{P}{v(P^0 - P)} = \frac{1}{V_m c} + \frac{(c-1)P}{V_m c} \cdot P^0 \tag{3.1}$$

3.2.2   Temperature programmed desorption

Ammonia temperature programmed desorption (NH_3-TPD) was performed in order to determine the acidity of the catalysts. The experimental setup consisted of mass flow controllers (MFC), a differential scanning calorimeter (DSC) and a mass spectrometer (MS). The MFCs regulated the inlet gas flow, the DSC controlled the temperature and the mass spectrometer analyzed the composition in the outlet stream. A simplified schematic of the equipment is illustrated in Figure 3.1.

In each sample, 20 mg of catalyst was mixed with 50 mg of SiO_2 in order to provide a more stable gas flow through the tube. The SiO_2 contained no acid sites and was therefore completely inert during the experiments. The samples were first heated to 500 °C (with a ramp of 20 °C/min) in a flow of Ar. The temperature was kept at 500 °C for 1 h while the samples were treated with 6.83 % of O_2 in Ar. The temperature was then decreased to 80 °C (with a ramp of 20 °C/min) and the samples were stabilized in a flow of Ar for 30 min. Further, the samples were exposed to a flow of 384 ppm NH_3 in Ar at 80 °C for 3 h (adsorption phase). The samples were then treated in a flow of Ar at 80 °C for 3 h to remove any physically adsorbed NH_3. The temperature was then increased to 600 °C (with a ramp of 10 °C/min) (desorption phase). When the temperature reached 600 °C it was further decreased to 20 °C (with a ramp of 20 °C/min).
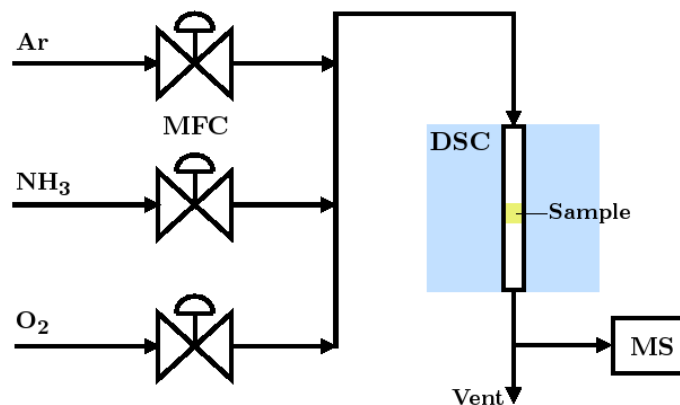
Figure 3.1: Simplified schematic of the equipment used for NH_3-TPD.

3.2.3 X-Ray Diffraction

The Y zeolites were analyzed by X-Ray Diffraction (XRD) to investigate the crystallinity of the materials. Prior to analysis, the zeolites were calcined in 550 °C for 6 h (with a ramp of 5 °C/min). The analysis was performed using a Siemens D5000 X-Ray Diffractometer, a picture of the equipment is shown in Figure 3.2.
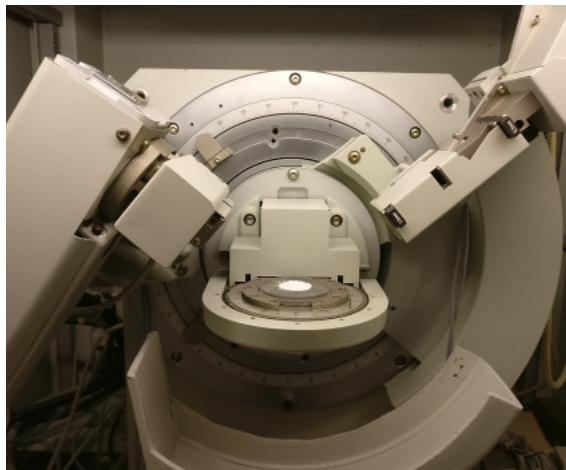
Figure 3.2: The equipment used for the XRD analysis.

3.2.4 Elemental microanalysis

The spent catalysts were analyzed by elemental microanalysis to determine the amount of carbon deposited onto the material during the reactions. Carbon content was determined by combustion of the samples at 1000 °C in the presence of oxygen. The gaseous combustion products were then separated in a column and quantitatively measured by a thermal conductivity detector (TCD).

3.3 Reaction experiments

The activity and selectivity of the prepared catalysts were evaluated by performing hydrodeoxygenation in a batch reactor at 320 and 345 °C and 50 bar of H_2 pressure.

3.3.1 Reactor setup

The hydrodeoxygenation reaction experiments were carried out in a 300 mL stainless steel batch reactor from Parr Instrument. A picture and schematic illustration of the reactor system is shown in Figure 3.3.
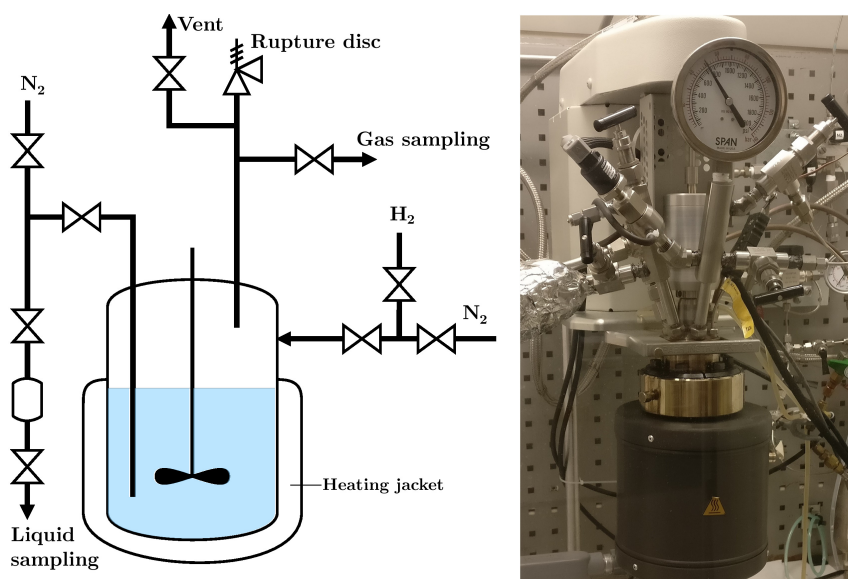
Figure 3.3: Schematic of the reactor setup used for the reaction experiments.

A gas line is connected to the reactor in order to either introduce hydrogen for the reactions or to purge the system with nitrogen. The reactor is equipped with two sampling lines, one for gas sampling and one for liquid sampling. A stirrer is fitted to the reactor in order to achieve good mixing of the reaction mixture and a heat jacket is enclosed around the vessel to provide heat. The reactor is also equipped with a cooling system where tap water can be circulated to cool the reactor internally. For safety reasons, the reactor is also equipped with a rupture disc to prevent the pressure from exceeding the maximum design pressure.

3.3.2   Catalyst activation process

Prior to all reaction experiments, the catalysts were activated through a sulfidation process. The sulfidation process was performed in the Parr instruments reactor. The standard procedure was to activate 500 mg of catalyst by 0.5 mL of dimethyl disulfide (DMDS) with 25 bar of hydrogen at 340 °C for 4 h. The amount of DMDS was in excess in order to achieve a full sulfidation of both the metal phases. The reactor was then cooled down and the catalyst was left in a nitrogen atmosphere until the following HDO experiments to prevent oxidation.

3.3.3   HDO experiments

The reactor was loaded with 500 mg of catalyst and a feed containing approximately 5.75 g (5 mol%) of 2-Phenethyl phenyl ether in 125 mL dodecane. Further, 0.1 mL of DMDS was also added to keep the catalyst in its sulfided form. The reactor was then sealed and purged three times with nitrogen followed by three times with hydrogen. The reactor was then pressurized to 10.5 bar with hydrogen and the stirring was set to 40-50 rpm. The heater was then started, and the reactor was

slowly heated to the operating temperature of 320-345 °C. When the temperature reached the desired value, the reactor was pressurized with 50 bar of hydrogen and the stirrer was set to 1000 rpm. The time when the reactor was pressurized to 50 bar was set as the starting time of the reaction experiments.

The reactions proceeded for a total of 6 h and liquid sampling was performed after 15, 35 and 60 minutes and then for every hour until the reactor was shut down. In total, eight samples were taken during the reaction experiments. The liquid sampling was performed by releasing approximately 0.6 bar of pressure through the sampling valve and then releasing it into a vial. Approximately 2 mL of liquid was sampled each time. Prior to each sampling the sampling line was flushed by releasing approximately 0.6 bar of pressure through the sampling valve and then flushing it with nitrogen. After each sampling the pressure in the reactor was restored to the operating pressure (50 bar) by adding hydrogen.

When the reactions had proceeded for 6 h the reactor heating system and the stirring was turned off. The reactor was then cooled down and depressurized slowly. The spent catalyst was retrieved and further filtered, washed with acetone and dried in 80 °C overnight.

3.4 Product sample analysis

The liquid samples were centrifuged (in a WIFUG Lab centrifuges 500 E) at 1500 rpm for 2 min in order to separate the catalyst particles from the liquid samples. 200 μL of sample was then put into a vial and analyzed by gas chromatography mass spectrometry (GC-MS). The products were identified by a (Agilent 5977A) mass selective detector and quantified by a (Agilent 7890B) gas chromatograph equipped with an HP-5 column and an Flame ionization detector (FID). During analysis, the oven was first kept at 100 °C for 1 min and was then heated to 190 °C (with a ramp of 10 °C/min) and further heated to 300 °C (with a ramp of 30 °C/min). The oven was then kept at 300 °C for 1.3 minutes. For quantification, the equipment was calibrated with external standards of cyclohexane, phenol, toluene, 2-phenethyl phenyl ether and ethylbenzene. Other peaks were quantified based on the closest related calibrated compound. The yield and selectivity of products were calculated according to Equation 3.2 and 3.3.

$$\text{Yield (mol\%)} = \frac{\text{Moles of product}}{\text{Moles of feed}} \cdot 100 \tag{3.2}$$

$$\text{Selectivity (\%)} = \frac{\text{Yield of product}}{\text{Total yield of products}} \cdot 100 \tag{3.3}$$

4

Results and discussion

In this chapter, the findings from the catalyst characterization and HDO experiments are presented and discussed. The catalysts were analyzed by nitrogen physisorption, XRD and NH_3-TPD. The influence of secondary mesoporosity, Si/Al ratio and temperature on the HDO performance is evaluated.

4.1 Catalyst characterization

4.1.1 Nitrogen physisorption

The prepared nonsulfided catalysts and catalyst support materials were analyzed by nitrogen physisorption to determine the surface area and pore structure. The nitrogen physisorption isotherms for the support materials are shown in Figure 4.1a and 4.2a.
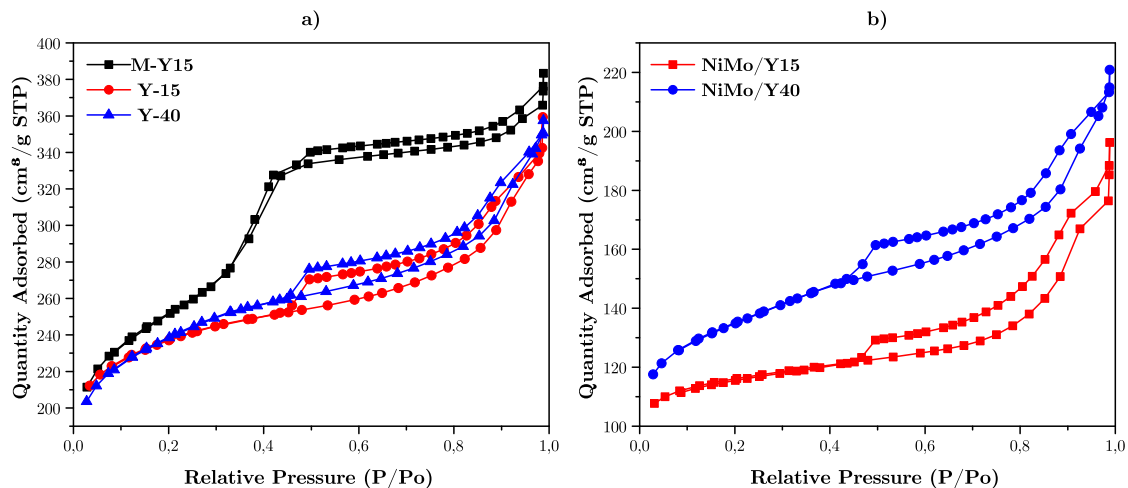
Figure 4.1: Adsorption and desorption isotherms. (a) catalyst support materials, (b) supported nonsulfided catalysts.

As can be seen, the isotherms for the modified support (M-Y15) is different from the parent, Y15. The parent Y15 shows a type II isotherm and the M-Y15 shows a type IV isotherm indicating it has a higher degree of ordered mesoporosity [42].

Y40 shows a similar isotherm to Y15 but is slightly shifted upwards, which indicates that it has a larger pore volume. The results from the analysis of Y2.6 are very far from the manufacturer's specification and the analysis was repeated with similar results. As can be seen in Figure 4.2a, Y2.6 shows an isotherm with a similar shape to Y15 and Y40 but is shifted very far down.

The isotherms for the supported catalysts are shown in Figure 4.1b and 4.2b. Unfortunately, no results for NiMo/M-Y15 is shown due to a shortage of sample. For NiMo/Y15 and NiMo/Y40, the isotherms are showing the same shape as for the supports but are shifted down slightly. This is most likely due to pore blockage from the NiMo impregnated on the surface, significantly reducing the pore volume. NiMo/Y2.6 however, shows a type III isotherm, which indicates that it has no or very little porosity and the nitrogen is only adsorbed on the outer surface [42]. This indicates that the impregnation of NiMo has blocked the majority of the pores in Y2.6. The Si/Al ratio of Y2.6 is very close to that of native Y zeolite and it is therefore expected to have very low mesoporosity. The extensive microporosity of the material increases the risk of pore blockage when impregnating metals, which can severely reduce the available porosity and surface area.
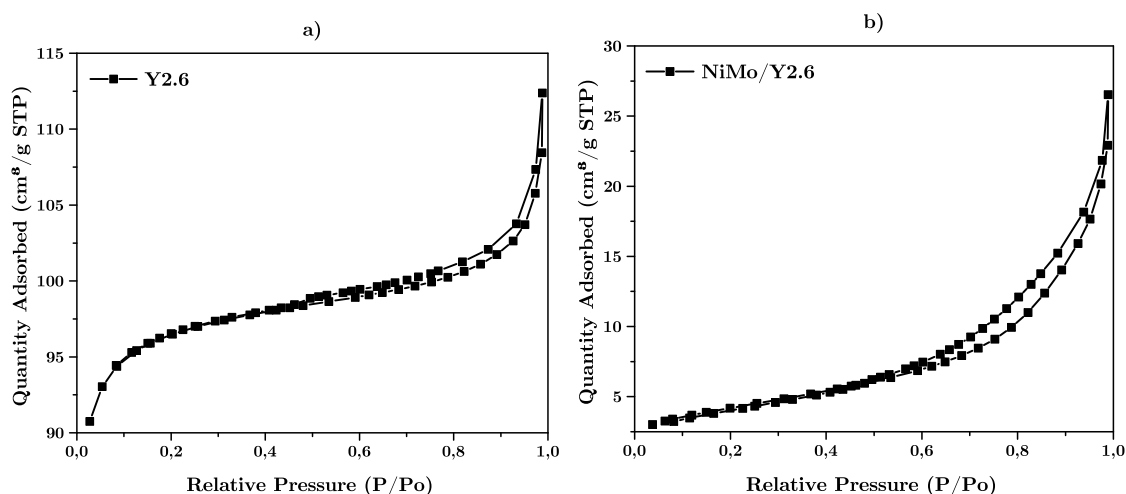
Figure 4.2: Adsorption and desorption isotherms. (a) Y2.6, (b) NiMo/Y2.6.

The BJH pore size distributions for the support materials are shown in Figure 4.3. As can be seen, the zeolite materials contain mostly pores with a size below 30 Å, Y2.6 contains only very small pores with a pore size less than 20 Å. The pore size distribution plot also shows that the surfactant-assisted modification of the zeolite has successfully introduced secondary mesoporosity in the range between 25 and 40 Å. The observations are consistent with results reported in other research where the method has been used [10, 36].
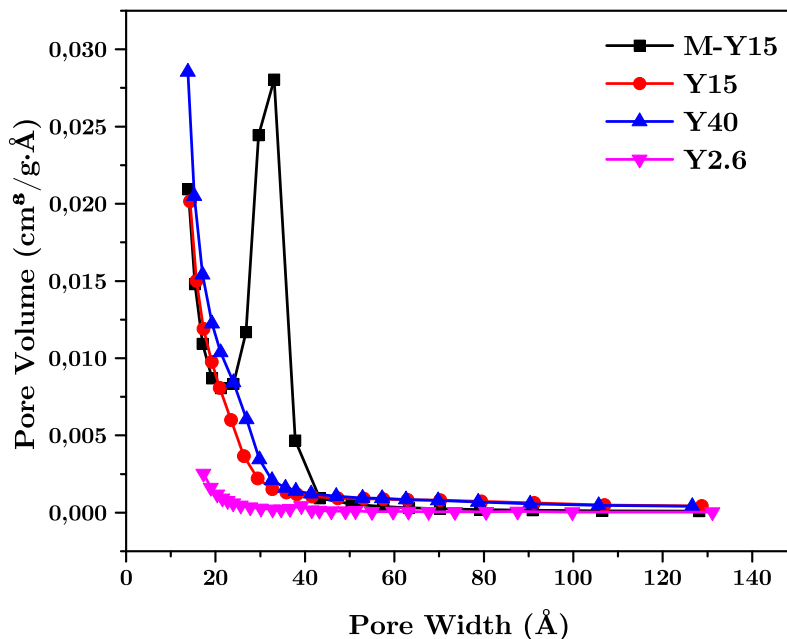
Figure 4.3: BJH pore size distributions of the different supports.

Table 4.1 contains information of the pore volume and surface area for both the supported catalysts and support materials. As mentioned, the results obtained from the analysis of Y2.6 were very different from the manufacturer's specifications. Nitrogen physisorption results for Y2.6 reported in the literature are also very different. Milena et al. have reported a BET surface area of 824 m^2g^{-1} and a total pore volume of 0.36 cm^3g^{-1} [43]. This suggests that the properties of Y2.6 have been altered in some way.

It can be seen from the results that with a higher grade of dealumination (higher Si/Al ratio) the mesopore volume and external surface area is increased. It can also be seen that when NiMo is impregnated on the support material the surface area and pore volume is significantly reduced. For NiMo/Y2.6, the majority of the BET surface area is represented by the external surface area, which suggests that almost all the pores are blocked in Y2.6.

Table 4.1: Data from the nitrogen physisorption analysis.

Material	Total pore volume cm^3/g	Micropore volume cm^3/g	Mesopore volume cm^3/g	BET surface area m^2/g	External surface area m^2/g
Y2.6	0.17	0.13	0.03	325	34
Y15	0.53	0.26	0.27	808	244
M-Y15	0.58	0.22	0.36	863	387
Y40	0.54	0.24	0.30	815	298
NiMo/Y2.6	0.04	0.00	0.04	15	14
NiMo/Y15	0.29	0.15	0.14	392	72
NiMo/Y40	0.33	0.14	0.20	462	164

As evident from Table 4.1, the surfactant-assisted modification has increased both surface area and pore volume. M-Y15 has a BET surface area of 863 compared to 808 m^2g^{-1} for the parent Y15. It also has an increased external surface area, 387 compared to 244 m^2g^{-1}. The mesopore volume is increased from 0.27 to 0.36 cm^3g^{-1}.

4.1.2 XRD

The diffraction patterns for the calcined Y zeolites are presented in Figure 4.4. The diffraction patterns correspond to the crystalline faujasite structure with only slightly shifted intensity [44]. When comparing Y15 and M-Y15 it is evident that the surfactant-assisted modification did not affect the crystallinity of the material to a great extent. The calcined Y2.6 however, shows much lower peak intensity compared to the other zeolites. To understand this behavior the diffraction patterns of calcined and non-calcined Y2.6 is shown in Figure 4.5.
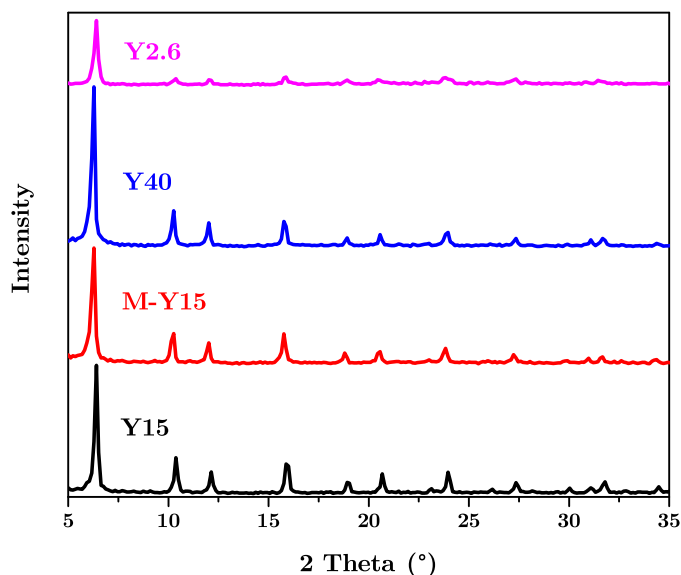
Figure 4.4: Diffraction patterns for the Y zeolites used in the study.

As the figure shows, the diffraction pattern has changed drastically by calcination treatment. The peaks for calcined Y2.6 is not as clear as in the non-calcined, which suggests that the Y2.6 is not thermally stable and the crystallinity is altered when calcined at 550 °C. This phenomenon could explain the strange results obtained by nitrogen physisorption, the calcination treatment most likely reduced the surface area of the Y2.6. The thermal stability of Y15 and Y40 should be higher since they have been dealuminated. However, it is unexpected that calcination at 550 °C can cause a significant deterioration in crystallinity of Y2.6.
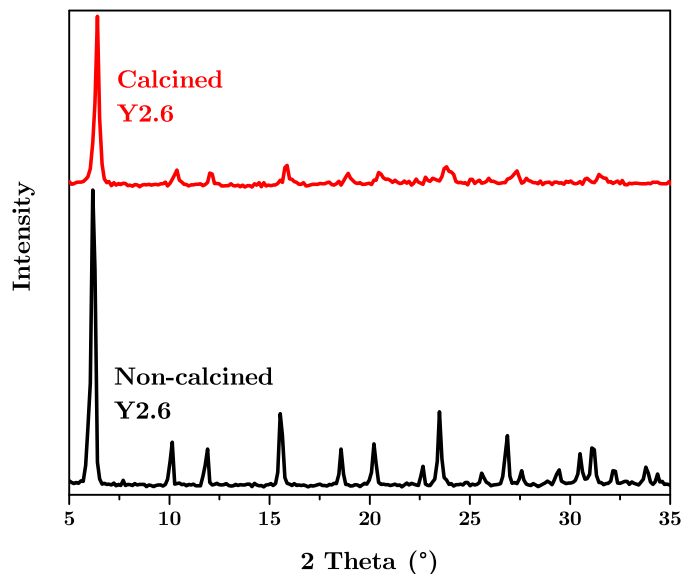
Figure 4.5: Diffraction patterns for calcined and non-calcined Y2.6.

4.1.3 TPD

The prepared catalysts were analyzed by NH_3-TPD to determine the amount and strength of acid sites. The desorption peaks are shown in Figure 4.6 and the total acidity is summarized in Table 4.2. As can be seen, the analysis of NiMo/Y2.6 resulted in no visible desorption peak, indicating that the material has none or very low acidity. The very low acidity is most likely related to the loss of crystallinity when the material is calcined as explained in Section 4.1.2. When the material is further loaded with NiMo the majority of the micropores are most likely blocked, severely limiting the ability of NH_3 to reach the active acid sites.

When the analysis was performed some problems were encountered. The zeolite-based catalysts form very fine particles and the catalyst powder seems to cause a pressure drop over the calorimeter tube, which further leads to misleading results in the MS. Therefore, the results from this analysis only show an indication of the trend in acidity of the catalysts and should be repeated for more accurate measurements.
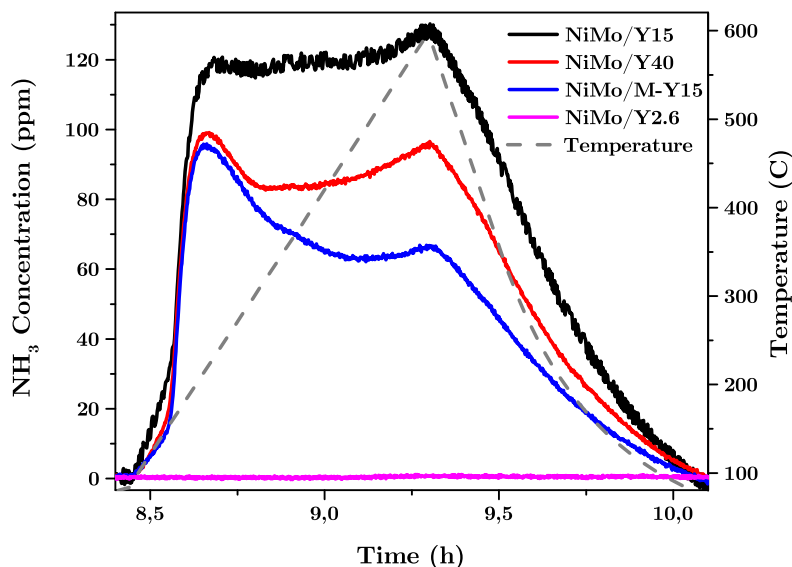
Figure 4.6: Concentration profiles of NH_3 in outlet gas stream during the desorption temperature ramp.

As can be seen from the figure, the peaks are hard to distinguish but it seems that the catalysts show one peak at around 220 °C and one at around 600 °C. NiMo/Y15 shows the highest total acidity and it seems that it has a high amount of both strong and weak acid sites. The catalyst supported on the modified Y15 shows a lower acidity compared to the catalyst supported on the parent Y15. It is apparent that the number of strong acid sites has been reduced to a greater extent since the peak at high temperature has been reduced more than the one at low temperature. This suggests that the surfactant-assisted modification has reduced the acidity of the zeolite which is in accordance with other reports where this treatment has been applied [45, 46].

The acidity of NiMo/M-Y15 however, seems to have been decreased more than expected. It is worth to note that, NiMo/M-Y15 produced the most severe pressure drop and therefore the acidity might be underestimated for this sample. NiMo/Y40 shows lower acidity compared to NiMo/Y15 which is probably due to the higher grade of dealumination in Y40 (higher Si/Al ratio) [39].

Table 4.2: Acid site density of the prepared catalysts.

Catalyst	mmol NH_3 g^{-1}
NiMo/Y2.6	-
NiMo/Y15	0.36
NiMo/M-Y15	0.21
NiMo/Y40	0.26

4.2   HDO of PPE

HDO of PPE involves a complex reaction network and yields a wide spectrum of different products. Figure A.1 and A.2 in Appendix A shows two typical GC-MS chromatograms from liquid sample analysis. From the GC-MS analysis of product samples with support from earlier reports in the literature a simplified reaction scheme for HDO of PPE is suggested in Figure 4.7 [15, 17, 47].
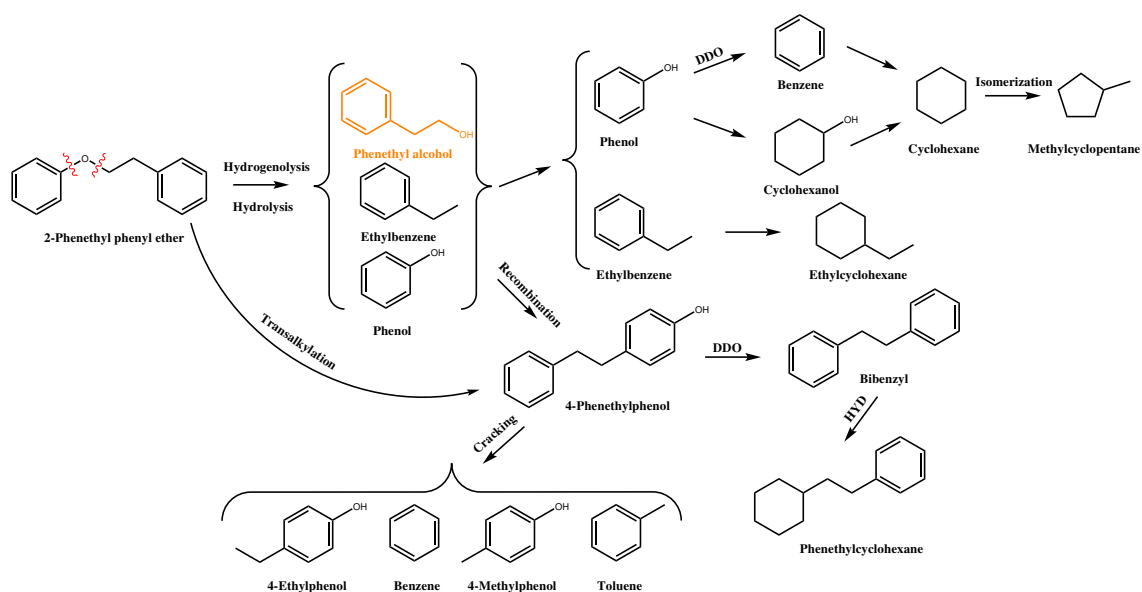
Figure 4.7: Suggested possible pathways for HDO of PPE.

The ether linkage in PPE is believed to be cleaved via two different routes, either through hydrogenolysis on metal sites or by acid catalyzed hydrolysis. The former produces ethylbenzene and phenol and the latter produces phenethyl alcohol and benzene. Phenethyl alcohol was, however, never detected in the product samples either due to it being converted very fast or that the hydrogenolysis route is more favoured. Further, phenol can be deoxygenated into benzene or cyclohexane through two different pathways and ethylbenzene can be hydrogenated into ethylcyclohexane. Cyclohexane can further undergo isomerization to produce methylcyclopentane.

Phenethylphenol (PEP) is also produced during HDO of PPE. This mechanism is not fully understood, but PEP is believed to be produced from transalkylation of PPE. In this reaction, the ethylbenzene side-chain in PPE is believed to be transferred to the phenolic ring to produce PEP. It is also suggested to be a product from recombination of ethylbenzene and phenol. PEP is an interesting intermediate since it consist of a relatively stable C-C linkage. However, this is an undesired product if the goal is to produce monoaromatics and monocyclic compounds. PEP can be further depolymerized through cracking of the C-C linkage to produce benzene and ethylphenol or ethylbenzene and methylphenol. PEP can also be deoxygenated to produce bibenzyl, which can be further hydrogenated into phenethylcyclohexane.

When analyzing the liquid product samples in GC-MS, some minor peaks with high retention time appeared. These products were not possible to identify in a good manner and when quantified using the calibration for PPE they only constitutes approximately 1-2 % of the selectivity. Since these compounds could not be identified and seem to be of very low quantities, they are excluded from the analysis presented here.

4.2.1 Influence of secondary mesoporosity

In order to investigate the effect of introducing secondary mesoporosity into Y15, reaction experiments were performed. PPE was treated over the two catalysts, NiMo/M-Y15 and NiMo/Y15 at 320 and 345 °C and 50 bar H_2.

4.2.1.1 Conversion

At 320 °C, both catalysts effectively cleaved the β-O-4 linkage in PPE and full conversion (>99 %) was reached after 4 h. Figure 4.8a shows the conversion during the experiments. As can be seen, the catalyst supported on the modified Y15 shows a slightly higher conversion rate, which might be explained by the higher mesopore volume and surface area of the catalyst. The experiment was then repeated at a higher temperature of 345 °C and as expected, the conversion rate increased and full conversion was reached for both catalysts after 3 h. However, as can be seen from Figure 4.8b the modified support shows only a very small increase in the rate of conversion at this temperature.
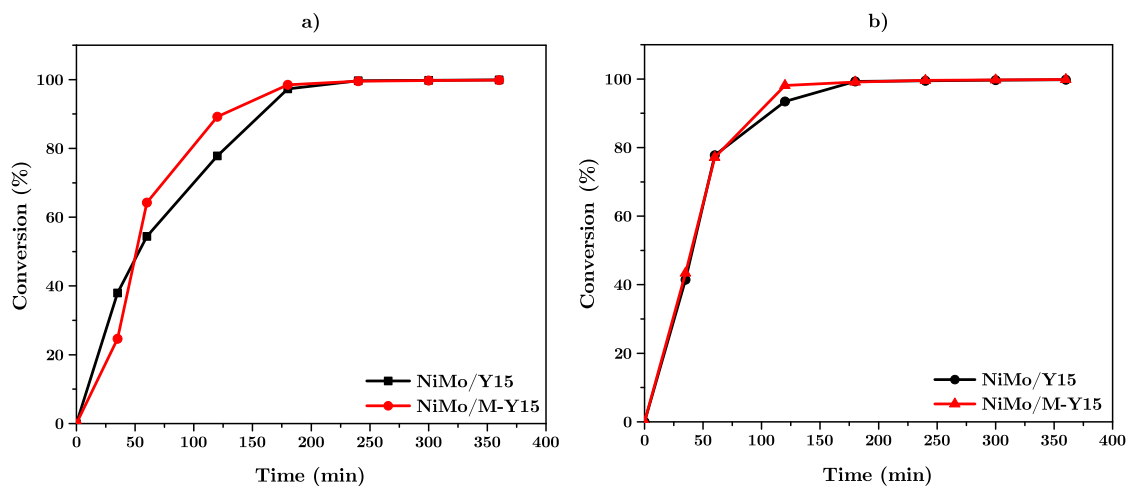
Figure 4.8: Conversion of PPE over time for NiMo/Y15 and NiMo/M-Y15. (a) 320 °C, (b) 345 °C.

4.2.1.2 Product selectivity

The product selectivity of the catalysts is shown in Figure 4.9. The products are divided into three groups: cycloalkanes, deoxygenated aromatics and phenolics. More detailed selectivity data is presented in Appendix B. It can be seen that the two catalysts show similar selectivity of products, however, the selectivity for cycloalkanes and deoxygenated aromatics is lower and the selectivity for phenolics is higher for NiMo/M-Y15. The trend is similar for both of the reaction temperatures. This indicates that the catalyst supported on the modified zeolite shows slightly lower HDO activity. Earlier research suggests that acid sites can improve deoxygenation activity and therefore, a reason for the lower activity could be due to the lower acidity of NiMo/M-Y15. Another possible reason for the varying activity could be differences in the dispersion of the NiMo phase on the two supports due to their different pore structure. This was, however, not analyzed in this study.
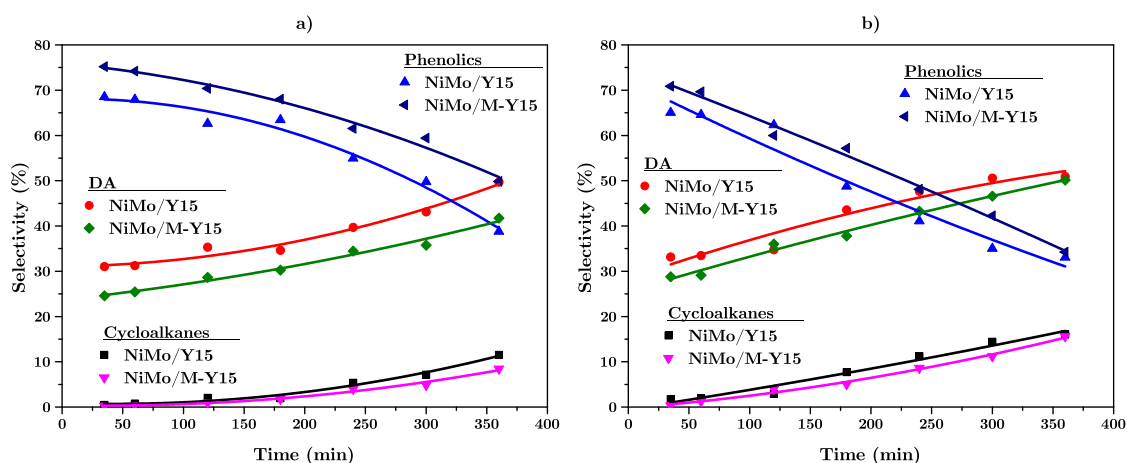
Figure 4.9: Product selectivity of cycloalkanes (CA), deoxygenated aromatics (DA) and phenolics (PH). (a) 320 °C, (b) 345 °C.

Figure 4.10 shows the yield of dimers containing C-C linkages, more specifically PEP and bibenzyl. It is evident from the plot that the formation of dimers, as well as the cleavage of the formed C-C linkages, is affected by the different properties of the modified and non-modified support. PEP formation is faster on NiMo/M-Y15 at both temperatures but the formation of bibenzyl is almost identical for both catalysts. The higher rate of PEP formation is most likely related to the higher conversion rate of PPE for NiMo/M-Y15. The cracking of C-C linkages appears to be slightly slower over NiMo/M-Y15 for both reaction temperatures.

A reasonable explanation of this behaviour could be that the higher pore size and pore volume in the modified support material makes it more selective for dimer formation. The secondary mesoporosity in NiMo/M-Y15 most likely makes it easier for PPE to reach the active acid sites that catalyze transalkylation. NiMo/Y15 has higher acid site density but the larger mass transport resistance in the catalyst might limit the rate of transalkylation. The slower cracking of C-C linkages can be related

to the low amount of strong acid sites in NiMo/M-Y15 compared to NiMo/Y15 since
the strong acid sites are responsible for the cleavage of such linkages. The lower
cracking activity of NiMo/M-Y15 can also cause more dimer accumulation and thus
higher peak concentration of PEP. Acidity should promote PEP formation, but it
seems that the strong acid sites that were removed in the modification treatment
were more important for cracking reactions than for dimer formation.
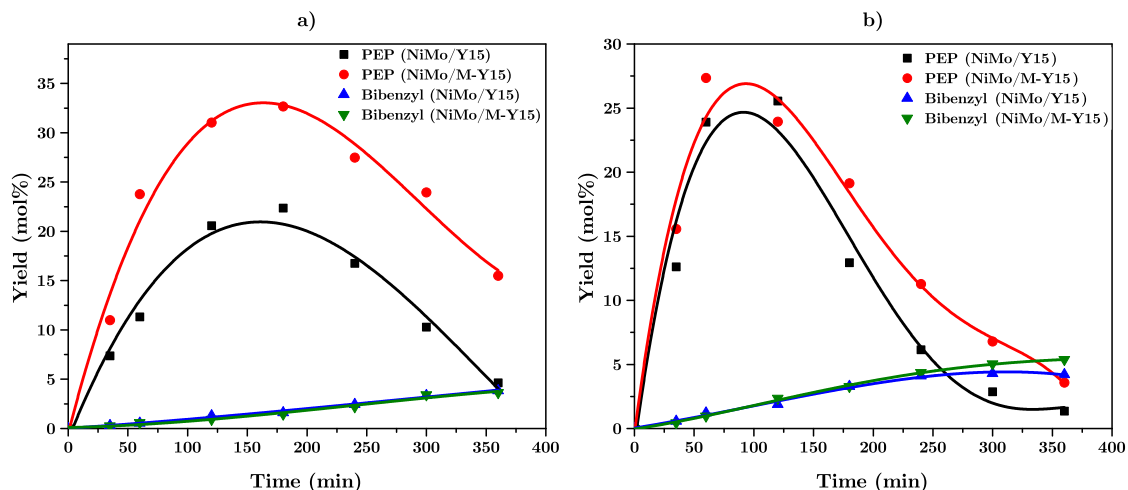
Figure 4.10: Yield of dimers containing C-C linkages during the experiment. (a)
320 °C, (b) 345 °C.

4.2.2 Influence of Si/Al ratio

NiMo supported on three Y zeolite supports with different Si/Al ratio were used
for HDO of PPE to investigate how the selectivity and activity is influenced by the
varying support properties. PPE was treated with 50 bar of hydrogen at 345 °C for
6 h.

4.2.2.1 Conversion

All catalysts were able to cleave the β-O-4 bond in PPE to produce ethylbenzene
and phenol. Figure 4.11 shows the conversion of PPE over time for the different
catalysts. As can be seen, the conversion rate is lowest for NiMo/Y2.6 which is
not reaching full conversion even after 6 h. The slow conversion might be related
to the low available external surface area, acidity and loss of crystallinity in the
zeolite support. NiMo/Y15 is fastest in converting PPE but only slightly faster
than NiMo/Y40.
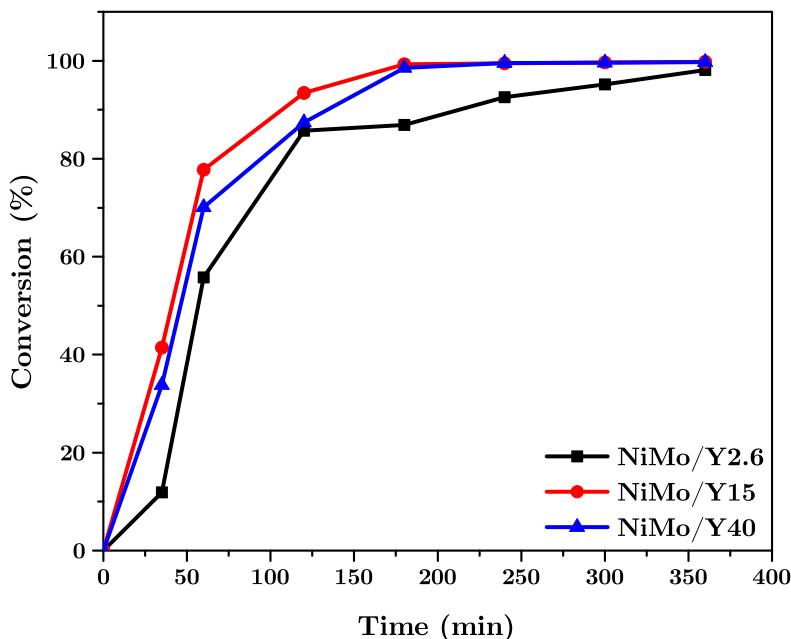
Figure 4.11: Conversion of PPE over time for the different catalysts.

NiMo/Y40 shows lower conversion rate compared to NiMo/Y15 even though it has both a higher BET surface area and mesopore volume. This suggests that the conversion is also related to the acidity of the catalyst. As mentioned, acid sites can catalyze transalkylation reactions and produce PEP from PPE. The lower acidity of Y40 might be related to a lower rate of transalkylation and therefore a slower conversion of PPE.

4.2.2.2 Product selectivity

The selectivity of products for the three different catalysts is shown in Figure 4.12. It is apparent that the selectivity is changing with different Si/Al ratio. The results imply that both pore structure and acidity plays an important role in converting PPE into valuable products. NiMo/Y15 shows a lower selectivity for phenol and higher selectivity towards cycloalkanes and benzene compared to the other catalysts, which suggests that the catalyst is more active for phenol HDO. The higher selectivity for phenol and lower selectivity for cycloalkanes in NiMo/Y40 and NiMo/Y2.6 is most likely related to their lower acidity compared to NiMo/Y15. Another possible explanation could be differences in the dispersion of the NiMo phase, which was not analyzed in this study.
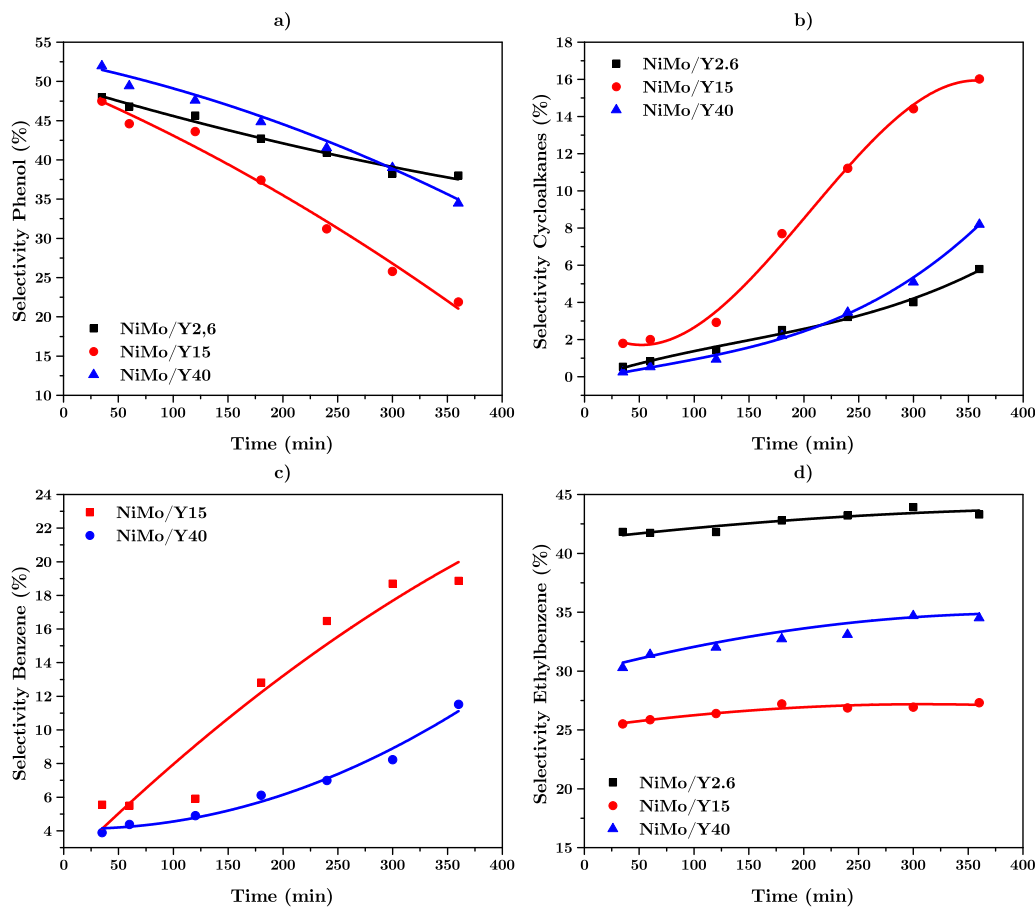
Figure 4.12: Selectivity of products for the different catalysts. (a) Phenol, (b) Cycloalkanes, (c) Benzene, (d) Ethylbenzene.

The selectivity of products after 6 h reaction time is shown in Table 4.3. NiMo/Y2.6 produces no benzene and is the only catalyst producing cyclohexanol. This result implies that it is active for the second pathway of phenol HDO where cyclohexanol is an intermediate as described in Section 2.2.1. NiMo/Y2.6 also shows no selectivity of methylcyclopentane while both NiMo/Y15 and NiMo/Y40 seems to convert all of the cyclohexane into methylcyclopentane. This is most likely due to the low acidity of NiMo/Y2.6, earlier research suggests that skeletal isomerization reactions require strong acid sites which is present in NiMo/Y15 and NiMo/Y40 [48].

Table 4.3: Selectivity of products after 6 h.

| Species	Selectivity (%)		
	NiMo/Y2.6	NiMo/Y15	NiMo/Y40
Methylcyclopentane	-	10.8	7.7
Cyclohexane[1]	5.8	5.2	0.5
Benzene	-	18.9	11.5
Ethylbenzene	43.3	27.3	34.5
Toluene	2.2	2.5	1.7
Cyclohexanol	4.0	-	-
Phenol	38.0	21.9	34.5
Ethylphenol	-	10.4	2.4
Phenethylphenol (PEP)	5.9	0.7	5.5
Bibenzyl	0.2	2.2	1.6
Phenethylcyclohexane	0.59	-	-

[1] Includes Methylcyclohexane, Dimethylcyclohexane and Ethylcyclohexane

As evident from Figure 4.12d and Table 4.3, the selectivity of ethylbenzene is different when comparing the catalysts. They all show the same trend and maintain a stable selectivity throughout the whole reaction time. The selectivity of ethylbenzene is strongly related to the selectivity of transalkylation and recombination reactions. Ethylbenzene is formed when PPE is cleaved through hydrogenolysis and if the transalkylation route is more favoured, less ethylbenzene will be formed. It also depends on the rate of recombination reactions, if recombination occurs to a large extent, less ethylbenzene will be present in the product samples.

Figure 4.13a shows the yield of PEP during the experiments. As can be seen, Ni-Mo/Y15 is more active for dimer formation which relates to NiMo/Y15 also showing the lowest selectivity towards ethylbenzene. NiMo/Y2.6 shows the opposite behaviour, high selectivity of ethylbenzene and low yield of dimers. NiMo/Y40 shows a higher rate of dimer formation than NiMo/Y2.6 but lower compared to NiMo/Y15. NiMo/Y40 has higher mesopore volume than NiMo/Y15, which should improve the diffusion of PPE to the active acid sites. However, as mentioned in Section 2.3.1.1, earlier research suggests that some of the mesopores in USY zeolite are connected through micropores and therefore the diffusion limitations of NiMo/Y40 and Ni-Mo/Y15 could be relatively similar. The lower rate of transalkylation reactions on NiMo/Y40 is therefore most likely related to the lower acidity of the catalyst.
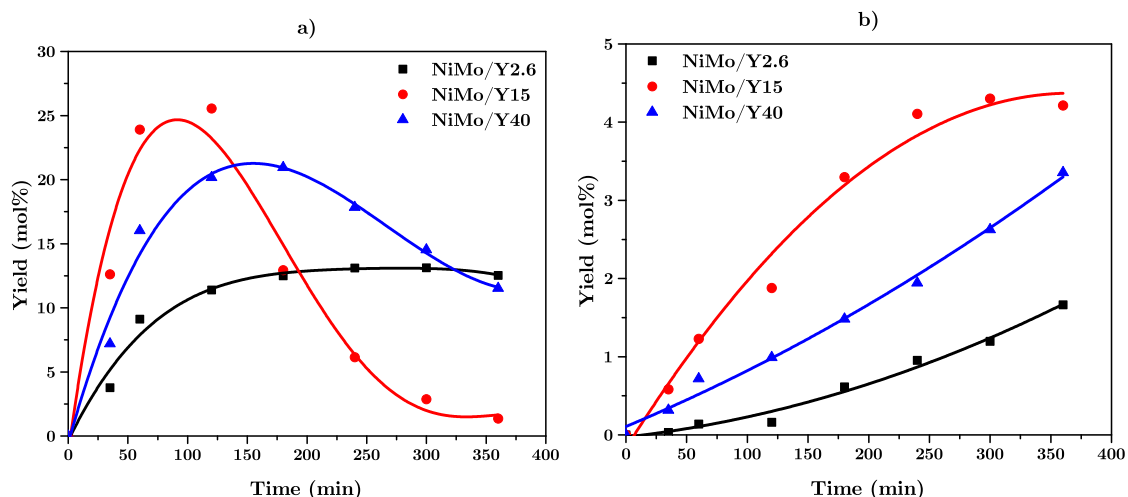
Figure 4.13: Yield of dimers containing C-C linkages. (a) PEP, (b) Deoxygenated aromatic dimers.

It can also be seen that the conversion of PEP is different over the catalysts. The catalysts are showing the same behaviour as for the production of PEP, NiMo/Y15 is fastest in converting PEP followed by NiMo/Y40 and NiMo/Y2.6. NiMo/Y2.6 is not showing a decrease in PEP even after 6 h, which most likely is related to the slow conversion of PPE over the catalyst. PEP is believed to be formed only when PPE is converted and since PPE is not fully converted over NiMo/Y2.6 even after 6 h, it is producing PEP during the whole experiment. NiMo/Y15 and NiMo/Y40 are, however, fully converting PPE after 3 h and therefore shows a significant decrease in PEP yield during the last hours.

As can be seen in Table 4.3 NiMo/Y2.6 produces no ethylphenol, indicating that the C-C linkage in PEP is not cleaved over the catalyst. The absence of cracking can be explained by the low acidity of NiMo/Y2.6. However, both NiMo/Y15 and NiMo/Y40 successfully cleave the C-C linkage in PEP. NiMo/Y15 is more active for cracking which might relate to the larger number of acid sites in the catalyst compared to NiMo/Y40.

Figure 4.13b shows the yield of bibenzyl and phenethylcyclohexane. NiMo/Y15 shows the highest yield of deoxygenated aromatic dimers followed by NiMo/Y40. NiMo/Y2.6 also shows a relatively high yield of deoxygenated aromatic dimers. However, it is important to note that cracking of the dimers is likely occurring on NiMo/Y15 and NiMo/Y40 and most likely not on NiMo/Y2.6. This gives a false impression that NiMo/Y2.6 is relatively fast in HDO of PEP. The rate of formation of these dimers is strongly related to the rate of PEP formation. It is, therefore, hard to relate the formation of deoxygenated aromatic dimers to HDO activity.

4.2.3   Influence of temperature

The effect of temperature on dimer formation and cracking of C-C linkages was investigated by comparing experiments performed at 320 °C and 345 °C using Ni-Mo/Y15. Figure 4.14 shows the yield of PEP and DA dimers for the two reaction temperatures. It is evident from the results that the rate of PEP formation is increased at a higher temperature but the rate of cracking reactions is not affected as much, which results in a higher peak yield of PEP at higher temperature. If the goal is to produce monomeric products from PPE it seems a lower temperature is more favorable since it still cleaves the C-C linkages but is less prone to form dimers.
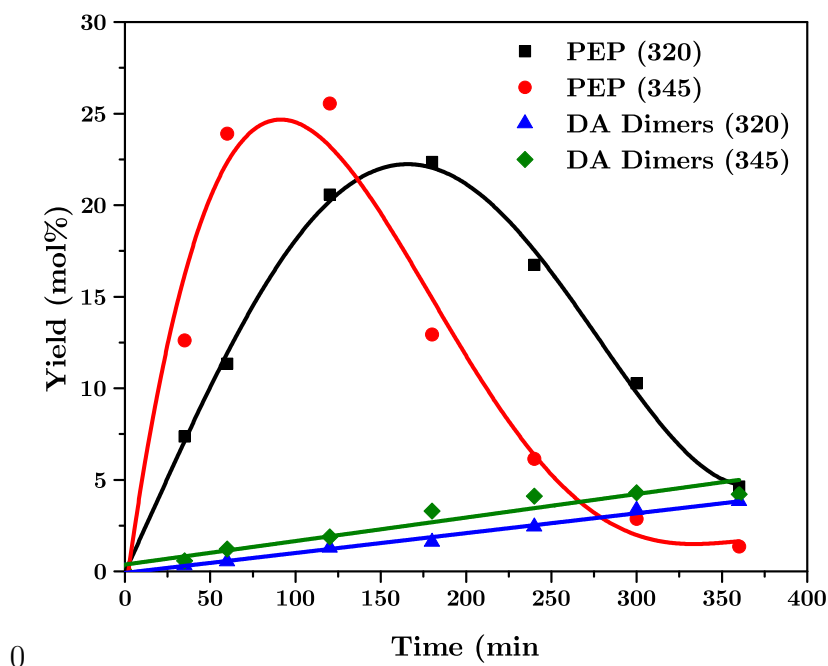
Figure 4.14: Yield of C-C dimers for NiMo/Y15 at 320 °C and 345 °C.

4.2.4   Catalyst deactivation

The spent catalysts were analyzed by elemental microanalysis to investigate how support properties influence coke formation. Table 4.4 shows the percentage of carbon in each of the spent catalysts used for PPE HDO at 345 °C.

Table 4.4: Carbon in spent catalysts according to elemental microanalysis.

Catalyst	Carbon content (%)
NiMo/Y2.6	1.10
NiMo/Y15	4.91
NiMo/M-Y15	4.46
NiMo/Y40	6.28

33

The spent NiMo/Y2.6 catalyst only contains 1,1 % carbon which might relate to the low activity of the catalyst. Coke formation is highly related to strong acid sites and cracking reactions and the low carbon deposition is possibly related to the very low acidity and absence of cracking. The spent NiMo/M-Y15 shows slightly lower coke deposition compared to NiMo/Y15, this is also most likely related to the lower acidity of the catalyst as NH_3-TPD suggests. NiMo/Y40 shows the highest coke deposition even though the results indicate that less cracking occurs over the catalyst compared to NiMo/Y15. This could be due to experimental error or that the different pore structure of Y40 is more selective for polymerization and polycondensation reactions.

4.3   Final discussion

The results imply that by using a bifunctional catalyst with the correct support properties, both β-O-4 and relatively strong C-C linkages can be cleaved effectively. However, the active sites that are responsible for the cracking reactions, also catalyze possibly problematic side reactions such as transalkylation and recombination reactions. As mentioned, these side reactions are likely not wanted when the goal is to produce monomeric aromatics and monocyclic compounds. However, if longer carbon chains are also of interest then this might provide an interesting pathway to increase the yield of dimeric products from lignin.

The products after 6 h reaction time still contain high amounts of phenolic compounds for all catalysts, which implies that the deoxygenation function of these catalysts needs to be improved to produce more valuable products such as renewable fuels. An alternative could be to further treat the products in a downstream process with a catalyst more active for deoxygenation to convert the residual phenolics.

5
Conclusions

Bifunctional NiMo catalysts were synthesized using different Y zeolite supports and further characterized by several techniques and studied for the HDO of PPE. Secondary mesoporosity was successfully introduced into Y zeolite with Si/Al of 15 by using a surfactant-assisted post-treatment. The study has shown that the properties of the zeolites seem to have a major impact on the activity and selectivity of the catalysts.

- The surfactant modification resulted in a significant increase of mesopores, retained crystallinity and lowered acidity. The catalyst supported on the modified support showed reduced HDO activity and increased selectivity for dimer formation compared to the catalyst supported on the non-modified support. The lower acidity is believed to be the reason for the lower HDO activity and the larger pore size is believed to make the catalyst more active for transalkylation and/or recombination reactions. Also, the lower acidity of the modified support had a greater influence on the rate of cracking reactions than on dimer formation, which resulted in a higher peak yield of dimers.

- Catalysts supported on Y zeolites with different Si/Al ratios resulted in varying activity and selectivity for HDO of PPE. Characterization of the catalysts showed varying properties such as acidity and pore structure. The results indicate that acidity has the largest impact on HDO of PPE. NiMo supported on Y zeolite with Si/Al of 15, showed the highest HDO activity and selectivity for cycloalkanes and deoxygenated aromatics.

- Temperature seems to have a large influence on dimer formation. The results suggest that the rate of dimer formation increases more with temperature than the rate of cracking reactions.

- The rate of coking seems to be influenced by support properties. However, the coke deposition shows no clear relation to a specific property, which indicates that both acidity and pore structure most likely affects the rate of coking.

5. Conclusions

6

Recommendations for future work

Further experimental work is needed to validate the results and to get a deeper understanding of the mechanisms involved. The reaction experiments need to be repeated to exclude experimental error. Some suggestions for future work are listed below.

- The experiments with Y2.6 should be repeated with a more careful calcination treatment to keep the crystallinity of the material intact.

- Experiments with NiMo supported on zeolites with other Si/Al ratios should be performed to get a deeper understanding of how it influences the selectivity and activity of the catalyst. It could be of interest to use Y zeolite with a Si/Al ratio in between 2.55-15 and 15-40 to investigate if there is a more optimal Si/Al ratio than 15.

- It could be of interest to introduce secondary mesoporosity into Y15 with a more severe method, such as desilication, which should result in larger pores than the surfactant-assisted method. This would give more information regarding diffusion limitations.

- Reaction experiments should be performed under the same conditions with NiMo supported on an inert support material such as carbon or SiO_2. Also, reaction experiments should be performed with Y zeolite without NiMo. This would give more detailed information about what active phase is responsible for what reaction and also if an interplay of the acid and metal sites is important.

- Further experiments with other lignin model compounds should also be performed to investigate how the support properties influence the conversion of other linkages in lignin. It could be interesting to use a compound with a C-C linkage as the feed to investigate and isolate the cracking performance in more detail.

- Further characterization of the catalysts should be performed to investigate if the dispersion of the impregnated NiMo is influenced by the Si/Al ratio or secondary-mesoporosity. This can be performed using transmission electron

microscopy (TEM).

Bibliography

[1] P. Mortensen, J.-D. Grunwaldt, P. Jensen, K. Knudsen, A. Jensen, "A review of catalytic upgrading of bio-oil to engine fuels", *Applied Catalysis A: General* **2011**, *407*, 1–19.

[2] T. M. Sankaranarayanan, A. Berenguer, C. Ochoa-Hernandez, I. Moreno, P. Jana, J. M. Coronado, D. P. Serrano, P. Pizarro, "Hydrodeoxygenation of anisole as bio-oil model compound over supported Ni and Co catalysts: Effect of metal and support properties", *Catalysis Today* **2015**, *243*, 163–172.

[3] S. Chakraborty, V. Aggarwal, D. Mukherjee, K. Andras, "Biomass to biofuel: a review on production technology", *Asia-Pacific Journal of Chemical Engineering* **2012**, *7*, 254–262.

[4] T. Choudhary, C. Phillips, "Renewable fuels via catalytic hydrodeoxygenation", *Applied Catalysis A: General* **2011**, *397*, 1–12.

[5] H. Rasmussen in *Springer Handbook of Petroleum Technology*, (Eds.: C. S. Hsu, P. R. Robinson), Springer International Publishing, Cham, **2017**, pp. 1133–1140.

[6] A. Gutierrez, E.-M. Turpeinen, T.-R. Viljava, O. Krause, "Hydrodeoxygenation of model compounds on sulfided CoMo/γ-Al2O3 and NiMo/γ-Al2O3 catalysts; Role of sulfur-containing groups in reaction networks", *Catalysis Today* **2017**, *285*, 125–134.

[7] S. Gillet, M. Aguedo, L. Petitjean, A. R. C. Morais, A. M. D. Lopes, R. M. Lukasik, P. T. Anastas, "Lignin transformations for high value applications: towards targeted modifications using green chemistry", *Green Chemistry* **2017**, *19*, 4200–4233.

[8] M. Saidi, F. Samimi, D. Karimipourfard, T. Nimmanwudipong, B. C. Gates, M. R. Rahimpour, "Upgrading of lignin-derived bio-oils by catalytic hydrodeoxygenation", *Energy & Environmental Science* **2014**, *7*, 103–129.

[9] A. L. Jongerius, R. Jastrzebski, P. C. Bruijnincx, B. M. Weckhuysen, "CoMo sulfide-catalyzed hydrodeoxygenation of lignin model compounds: An extended reaction network for the conversion of monomeric and dimeric substrates", *Journal of Catalysis* **2012**, *285*, 315–323.

[10] D. P. Gamliel, B. P. Baillie, E. Augustine, J. Hall, G. M. Bollas, J. A. Valla, "Nickel impregnated mesoporous USY zeolites for hydrodeoxygenation of anisole", *Microporous and Mesoporous Materials* **2018**, *261*, 18–28.

[11] E. SJÖSTRÖM in *Wood Chemistry (Second Edition)*, (Ed.: E. SJÖSTRÖM), Academic Press, San Diego, **1993**, pp. 71–89.

[12] J. Zakzeski, P. C. A. Bruijnincx, A. L. Jongerius, B. M. Weckhuysen, "The Catalytic Valorization of Lignin for the Production of Renewable Chemicals", *Chemical Reviews* **2010**, *110*, PMID: 20218547, 3552–3599.

[13] A. Vishtal, A. Kraslawski, "Challenges in industrial applications of technical lignins", *Bioresources* **2011**, *6*, 3547–3568.

[14] D. D. Laskar, B. Yang, H. Wang, J. Lee, "Pathways for biomass-derived lignin to hydrocarbon fuels", *Biofuels Bioproducts and Biorefining* **2013**, *7*, 602–626.

[15] B. Guvenatam, O. Kursun, E. H. J. Heeres, E. A. Pidko, E. J. M. Hensen, "Hydrodeoxygenation of mono- and dimeric lignin model compounds on noble metal catalysts", *Catalysis Today* **2014**, *233*, 83–91.

[16] X. P. Li, G. Y. Chen, C. X. Liu, W. C. Ma, B. B. Yan, J. G. Zhang, "Hydrodeoxygenation of lignin-derived bio-oil using molecular sieves supported metal catalysts: A critical review", *Renewable & Sustainable Energy Reviews* **2017**, *71*, 296–308.

[17] X. Zhou, X.-Y. Wei, Y.-M. Ma, Z.-M. Zong, "Effects of reaction conditions on catalytic hydroconversion of phenethoxybenzene over bifunctional Ni/Hβ", *Asia-Pacific Journal of Chemical Engineering* **2018**, *13*, e2228 APJ-17-0629.R1, e2228.

[18] B. Gomez-Monedero, J. Faria, F. Bimbela, M. P. Ruiz, "Catalytic hydroprocessing of lignin β-O-4 ether bond model compound phenethyl phenyl ether over ruthenium catalysts", *Biomass Conversion and Biorefinery* **2017**, *7*, 385–398.

[19] H. Topsøe, B. S. Clausen, F. E. Massoth in *Catalysis: Science and Technology*, (Eds.: J. R. Anderson, M. Boudart), Springer Berlin Heidelberg, Berlin, Heidelberg, **1996**, pp. 1–269.

[20] I. Graça, J. M. Lopes, H. S. Cerqueira, M. F. Ribeiro, "Bio-oils Upgrading for Second Generation Biofuels", *Industrial & Engineering Chemistry Research* **2013**, *52*, 275–287.

[21] O. Şenol, E.-M. Ryymin, T.-R. Viljava, A. Krause, "Effect of hydrogen sulphide on the hydrodeoxygenation of aromatic and aliphatic oxygenates on sulphided catalysts", *Journal of Molecular Catalysis A: Chemical* **2007**, *277*, 107–112.

[22] W. Zhang, J. Chen, R. Liu, S. Wang, L. Chen, K. Li, "Hydrodeoxygenation of Lignin-Derived Phenolic Monomers and Dimers to Alkane Fuels over Bifunctional Zeolite-Supported Metal Catalysts", *ACS Sustainable Chemistry & Engineering* **2014**, *2*, 683–691.

[23] M. M. Ambursa, P. Sudarsanam, L. H. Voon, S. B. A. Hamid, S. K. Bhargava, "Bimetallic Cu-Ni catalysts supported on MCM-41 and Ti-MCM-41 porous materials for hydrodeoxygenation of lignin model compound into transportation fuels", *Fuel Processing Technology* **2017**, *162*, 87–97.

[24] S. Jin, Z. Xiao, l. Chuang, X. Chen, L. Wang, J. Xing, W. Li, C. Liang, "Catalytic hydrodeoxygenation of anisole as lignin model compound over supported nickel catalysts", *Catalysis Today* **2014**, *234*, 125–132.

[25] Y.-C. Lin, C.-L. Li, H.-P. Wan, H.-T. Lee, C.-F. Liu, "Catalytic Hydrodeoxygenation of Guaiacol on Rh-Based and Sulfided CoMo and NiMo Catalysts", *Energy & Fuels* **2011**, *25*, 890–896.

[26] W. Fu, L. Zhang, D. Wu, M. Xiang, Q. Zhuo, K. Huang, Z. Tao, T. Tang, "Mesoporous zeolite-supported metal sulfide catalysts with high activities in the deep hydrogenation of phenanthrene", *Journal of Catalysis* **2015**, *330*, 423–433.

[27] X. Zhu, L. L. Lobban, R. G. Mallinson, D. E. Resasco, "Bifunctional transalkylation and hydrodeoxygenation of anisole over a Pt/HBeta catalyst", *Journal of Catalysis* **2011**, *281*, 21–29.

[28] H. Wang, M. Feng, B. Yang, "Catalytic hydrodeoxygenation of anisole: an insight into the role of metals in transalkylation reactions in bio-oil upgrading", *Green Chem.* **2017**, *19*, 1668–1673.

[29] V. Komvokis, L. X. L. Tan, M. Clough, S. S. Pan, B. Yilmaz in *Zeolites in Sustainable Chemistry: Synthesis, Characterization and Catalytic Applications*, (Eds.: F.-S. Xiao, X. Meng), Springer Berlin Heidelberg, Berlin, Heidelberg, **2016**, pp. 271–297.

[30] M. Breysse, J. Portefaix, M. Vrinat, "Support effects on hydrotreating catalysts", *Catalysis Today* **1991**, *10*, 489–505.

[31] G. de la Puente, A. Gil, J. J. Pis, P. Grange, "Effects of Support Surface Chemistry in Hydrodeoxygenation Reactions over CoMo/Activated Carbon Sulfided Catalysts", *Langmuir* **1999**, *15*, 5800–5806.

[32] V. N. Bui, D. Laurenti, P. Delichère, C. Geantet, "Hydrodeoxygenation of guaiacol: Part II: Support effect for CoMoS catalysts on HDO activity and selectivity", *Applied Catalysis B: Environmental* **2011**, *101*, 246–255.

[33] A. Gutierrez, R. Kaila, M. Honkela, R. Slioor, A. Krause, "Hydrodeoxygenation of guaiacol on noble metal catalysts", *Catalysis Today* **2009**, *147*, Special Issue dedicated to Marc Jacques Ledoux on the occasion of his 60th birthday, 239–246.

[34] D. Verboekend, N. Nuttens, R. Locus, J. Van Aelst, P. Verolme, J. C. Groen, J. Pérez-Ramírez, B. F. Sels, "Synthesis, characterisation, and catalytic evaluation of hierarchical faujasite zeolites: milestones, challenges, and future directions", *Chem. Soc. Rev.* **2016**, *45*, 3331–3352.

[35] K. Li, J. Valla, J. Garcia-Martinez, "Realizing the Commercial Potential of Hierarchical Zeolites: New Opportunities in Catalytic Cracking", *ChemCatChem* **2014**, *6*, 46–66.

[36] J. García-Martínez, M. Johnson, J. Valla, K. Li, J. Y. Ying, "Mesostructured zeolite Y—high hydrothermal stability and superior FCC catalytic performance", *Catalysis Science & Technology* **2012**, *2*, 987–994.

[37] P. Levecque, D. W. Gammon, P. Jacobs, D. De Vos, B. Sels, "The use of ultrastable Y zeolites in the Ferrier rearrangement of acetylated and benzylated glycals", *Green Chem.* **2010**, *12*, 828–835.

[38] J. Weitkamp, M. Hunger, "Chapter 22 Acid and base catalysis on zeolites", *Studies in Surface Science and Catalysis - STUD SURF SCI CATAL* **2007**, *168*, 787–835.

[39] J. Huang, W. Long, P. K. Agrawal, C. W. Jones, "Effects of Acidity on the Conversion of the Model Bio-oil Ketone Cyclopentanone on H-Y Zeolites", *Journal of Physical Chemistry C - J PHYS CHEM C* **2009**, *113*, DOI `10.1021/jp905661w`.

[40] E. Furimsky, F. E. Massoth, "Deactivation of hydroprocessing catalysts", *Catalysis Today* **1999**, *52*, 381–495.

[41] J. Ross, *Heterogeneous Catalysis: Fundamentals and Applications*, Elsevier Science, **2012**.

[42] M. Thommes, K. Kaneko, A. V. Neimark, J. Olivier, F. Rodriguez-Reinoso, J. Rouquerol, K. Sing, "Physisorption of gases, with special reference to the evaluation of surface area and pore size distribution (IUPAC Technical Report)", *Pure and Applied Chemistry* **2015**, *87*, DOI `10.1515/pac-2014-1117`.

[43] M. Milina, S. Mitchell, J. Pérez-Ramírez, "Prospectives for bio-oil upgrading via esterification over zeolite catalysts", *Catalysis Today* **2014**, *235*, Recent developments in catalyst design and activation, 176–183.

[44] In *Collection of Simulated XRD Powder Patterns for Zeolites (Fifth Edition)*, (Eds.: M. Treacy, J. Higgins), Elsevier Science B.V., Amsterdam, **2007**, pp. 10–16.

[45] J. F. Silva, E. D. Ferracine, D. Cardoso, "Effects of Different Variables on the Formation of Mesopores in Y Zeolite by the Action of CTA+ Surfactant", *Applied Sciences* **2018**, *8*, DOI `10.3390/app8081299`.

[46] R. Chal, T. Cacciaguerra, S. van Donk, C. Gérardin, "Pseudomorphic synthesis of mesoporous zeolite Y crystals", *Chem. Commun.* **2010**, *46*, 7840–7842.

[47] Z. Luo, C. Zhao, "Mechanistic insights into selective hydrodeoxygenation of lignin-derived β-O-4 linkage to aromatic hydrocarbons in water", *Catal. Sci. Technol.* **2016**, *6*, 3476–3484.

[48] V. Kazansky, "The Catalytic Site from a Chemical Point of View", Studies in Surface Science and Catalysis **1994**, *85*, (Eds.: J. Jansen, M. Stöcker, H. Karge, J. Weitkamp), 251–272.
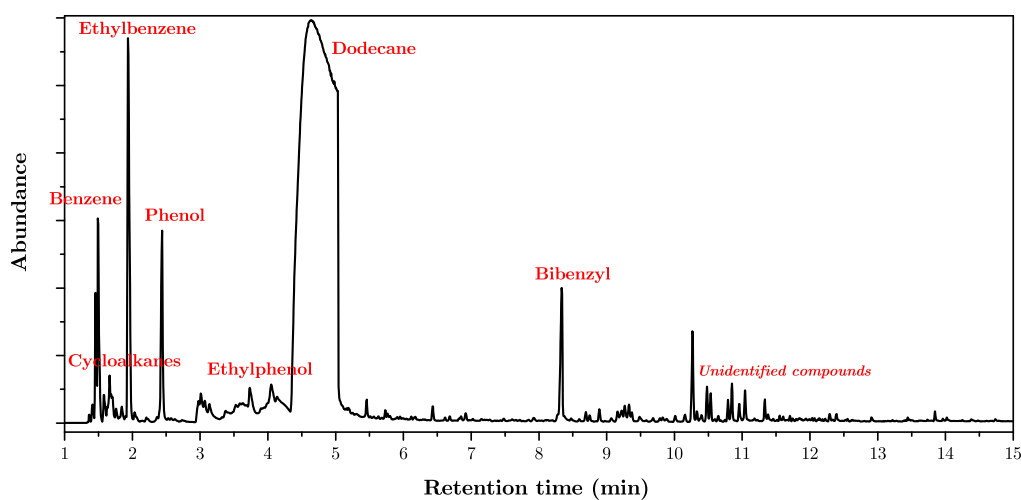
A

GC-MS Chromatograms

In this appendix typical chromatograms from liquid sample analysis are presented.
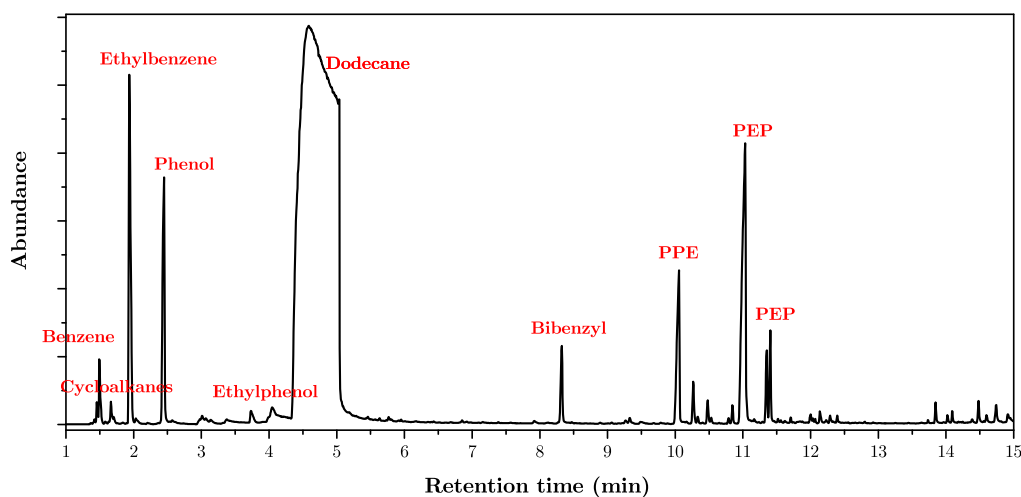
Figure A.1: GC-MS chromatogram of product sample after 2 h reaction time.

Figure A.2: GC-MS chromatogram of product sample after 6 h reaction time.

A. GC-MS Chromatograms

II

B

Selectivity data

In this appendix detailed selectivity data from the reaction experiments is presented.

B.1 NiMo/M-Y15 (320 °C)

Table B.1: Selectivity of products over time for NiMo/M-Y15 at 320 °C.

Species	Selectivity (%)						
	35	60	120	180	240	300	360
Methylcyclopentane	0.27	0.39	0.94	1.79	3.99	4.83	8.43
Benzene	3.26	2.76	3.90	4.71	7.47	7.97	12.43
Ethylbenzene	20.82	22.11	24.17	24.68	25.82	25.87	27.25
Phenol	49.60	46.48	46.48	43.80	41.66	38.17	35.84
Ethylphenol	5.59	4.98	4.10	5.35	5.13	8.08	5.30
Bibenzyl	0.48	0.57	0.59	0.83	1.18	1.89	2.05
Phenethylphenol	19.99	22.72	19.81	18.83	14.75	13.19	8.70

B.2 NiMo/Y15 (320 °C)

Table B.2: Selectivity of products over time for NiMo/Y15 at 320 °C.

Species	Selectivity (%)						
	35	60	120	180	240	300	360
Methylcyclopentane	0.47	0.78	2.05	1.93	5.36	7.16	11.53
Benzene	4.15	3.11	4.75	3.62	7.93	9.43	13.67
Ethylbenzene	25.37	26.73	29.06	29.36	29.62	30.41	32.89
Phenol	48.07	45.41	46.29	44.43	41.03	36.22	30.98
Ethylphenol	5.62	6.24	3.49	4.53	4.84	6.95	4.46
Cresol	0.00	0.00	0.30	0.36	0.51	0.87	1.03
Bibenzyl	0.64	0.78	0.79	1.01	1.25	1.86	1.91
Phenethylphenol	14.82	16.31	12.56	14.10	8.56	5.69	2.31

B.3 NiMo/M-Y15 (345 °C)

Table B.3: Selectivity of products over time for NiMo/M-Y15 at 345 °C.

Species	Selectivity (%)						
	35	60	120	180	240	300	360
Methylcyclopentane	0.34	0.66	2.97	3.75	6.51	8.28	11.71
Cyclohexane[1]	0.00	0.59	1.00	1.29	2.10	2.90	3.89
Benzene	4.25	3.67	7.85	8.47	12.60	14.59	18.45
Toluene	0.76	0.67	1.14	1.14	1.54	1.88	2.27
Ethylbenzene	23.18	24.01	25.64	26.03	26.46	27.13	26.59
Phenol	49.58	47.02	41.34	41.48	36.13	31.68	25.48
Ethylphenol	0.00	0.99	4.43	3.12	5.14	6.57	6.89
Bibenzyl	0.61	0.76	1.40	2.15	2.65	2.97	2.84
Phenethylphenol	21.29	21.63	14.22	12.57	6.86	4.01	1.89

[1] Includes Methylcyclohexane, Dimethylcyclohexane and Ethylcyclohexane

B.4 NiMo/Y15 (345 °C)

Table B.4: Selectivity of products over time for NiMo/Y15 at 345 °C.

Species	Selectivity (%)						
	35	60	120	180	240	300	360
Methylcyclopentane	0.80	1.08	1.88	5.71	8.19	10.26	10.85
Cyclohexane[1]	0.99	0.92	1.04	1.99	3.03	4.16	5.18
Benzene	5.55	5.50	5.92	12.81	16.48	18.69	18.86
Toluene	1.30	1.21	1.20	1.77	2.23	2.72	2.50
Ethylbenzene	25.51	25.86	26.39	27.20	26.86	26.94	27.31
Phenol	47.49	44.61	43.62	37.43	31.22	25.79	21.90
Ethylphenol	0.00	2.87	1.66	4.35	6.69	7.76	10.43
Bibenzyl	0.81	0.88	1.25	1.77	2.13	2.21	2.24
Phenethylphenol	17.55	17.07	17.05	6.96	3.18	1.48	0.72

[1] Includes Methylcyclohexane, Dimethylcyclohexane and Ethylcyclohexane

B.5 NiMo/Y40 (345 °C)

Table B.5: Selectivity of products over time for NiMo/Y40 at 345 °C.

	Selectivity (%)						
Species	**35**	**60**	**120**	**180**	**240**	**300**	**360**
Methylcyclopentane	0.25	0.49	0.87	2.10	3.34	4.78	7.78
Cyclohexane	0.00	0.05	0.07	0.13	0.20	0.31	0.49
Benzene	3.89	4.44	4.97	6.20	7.17	8.25	11.62
Toluene	1.21	1.22	1.16	1.21	1.33	1.61	1.75
Ethylbenzene	30.28	31.82	32.47	33.17	33.91	34.80	34.79
Phenol	51.97	50.06	48.26	45.45	42.56	39.13	34.76
Ethylphenol	0.00	0.37	0.46	0.49	0.95	1.34	1.61
Bibenzyl	0.52	0.50	0.55	0.74	1.04	1.50	1.62
Phenethylphenol	11.88	11.06	11.19	10.50	9.50	8.28	5.58

[1] Includes Methylcyclohexane, Dimethylcyclohexane and Ethylcyclohexane

B.6 NiMo/Y2.6 (345 °C)

Table B.6: Selectivity of products over time for NiMo/Y2.6 at 345 °C.

	Selectivity (%)						
Species	**35**	**60**	**120**	**180**	**240**	**300**	**360**
Methylcyclopentane	0.00	0.00	0.00	0.00	0.00	0.00	0.00
Cyclohexane	0.54	0.82	1.44	2.51	3.21	4.02	5.80
Benzene	0.00	0.00	0.00	0.00	0.00	0.00	0.00
Toluene	2.12	2.10	2.05	2.10	2.04	2.02	2.16
Ethylbenzene	41.82	41.74	41.81	42.79	43.22	43.92	43.30
Phenol	48.00	46.79	45.65	42.72	40.91	38.26	38.02
Ethylphenol	0.00	0.00	0.00	0.00	0.00	0.00	0.00
Cyclohexanol	2.14	2.52	2.76	3.23	3.34	3.50	4.01
Bibenzyl	0.02	0.04	0.03	0.09	0.13	0.17	0.20
Phenethylcyclohexane	0.02	0.05	0.06	0.22	0.36	0.52	0.59
Phenethylphenol	5.34	5.95	6.21	6.34	6.79	7.59	5.93

[1] Includes Methylcyclohexane, Dimethylcyclohexane and Ethylcyclohexane